Analysis of IRS-Assisted Downlink Wireless Networks Over Generalized Fading

Yunli Li and Young Jin Chun, *Member, IEEE*

***Abstract*— Intelligent Reflecting Surface (IRS) is a communication technology that can control the phase shift and reflection of the incoming signal towards the destination, achieving high spectral efficiency at a low hardware cost. However, the IRS-assisted wireless networks pose fundamental challenges on statistical channel modeling. Communication assisted by the IRS takes the form of a mixture channel, composed of a direct link and cascaded link aided by the IRS, which is often intractable to analyze, requires advanced functions, such as Meijer's G or Fox's H functions, to describe, and only applies to a certain operating frequency or network environment. These limitations motivate the development of a tractable and highly accurate channel model for IRS-assisted wireless networks, but versatile enough to be applied to any frequency band and communication scenario given proper parameterization. To this end, we utilize the mixture Gamma distributions to model IRS-assisted communication and derive distributions of the mixture channel for both multiplicability and quadratic form. The system performance of the IRS-assisted wireless network is analyzed using stochastic geometry, and the approximation accuracy of the proposed channel model is validated through extensive numerical simulation. These results indicate that the mixture Gamma distribution-based approximation can greatly facilitate the modeling and analysis in IRS-assisted networks with high accuracy.**

***Index Terms*— Intelligent reflecting surface, mixture Gamma distribution, cascaded channel, mixture channel, generalized fading, stochastic geometry.**

I. Introduction

SIXTH-GENERATION (6G) wireless communication systems, such as Terahertz (THz) systems, are expected to provide transformative solutions for a fully connected world by offering high capacity, massive connectivity, high reliability and low latency. However, as 6G systems move to higher frequencies, such requirements present significant challenges due to rapid attenuation and weak penetration [1]. One promising approach that has recently emerged is the concept of an intelligent communication environment (ICE), which introduces controllability to the wireless propagation medium through controlled reflection, absorption, and tuning [2].

One popular and practical technology to achieve ICE is the intelligent reflecting surface (IRS), also known as reconfigurable intelligent surface (RIS) or large-scale intelligent surface (LIS) [3], [4], [5]. IRS is composed of numerous passive reflecting elements on a planar surface and a control module that regulates the phase shift and radiation direction of each reflecting element. In contrast to conventional RF chains, the passive reflecting elements merely reflect signals without additional active processing, facilitating easy and cost-efficient deployment. Furthermore, the IRS often operates in noise-free mode without requiring additional self-interference cancellation compared to full-duplex relays. Therefore, IRS is a revolutionary technology that can achieve high spectral- and energy-efficient communications at a low cost.

A. Motivation

IRS-assisted transmission constructs a mixed channel composed of a direct link between the Base Station (BS) and User Equipment (UE), as well as a cascaded link across the BS, IRS, and UE. However, existing research faces challenges in statistically characterizing cascaded and mixed channels in IRS-assisted networks due to the involvement of advanced functions like Fox's H or Meijer's G functions, even for the simplest double-Rayleigh fading.

Furthermore, future wireless systems will operate in diverse environments, which often result in propagation characteristics that differ significantly from conventional Rayleigh fading [6]. These characteristics include the clustering of scattered multipath contributions, shadowing caused by obstacles or human movement, and random fluctuations of received signals. These phenomena can significantly degrade the end-to-end network performance as described in [7]. As such, it is essential to extend the analysis of IRS-assisted wireless communication systems to generalized fading.

Therefore, analyzing the performance of IRS-assisted wireless networks becomes challenging. Nevertheless, some studies have opted for moment matching methods to trade accuracy for tractability in channel modeling. Consequently, for evaluating the performance metrics of IRS-assisted systems, it is critical to propose a tractable approximation model for cascaded link and mixture channel with high accuracy, especially when each link follows a generalized fading distribution.

Manuscript received 13 May 2023; revised 14 August 2023 and 12 December 2023; accepted 8 February 2024. Date of publication 4 March 2024; date of current version 14 August 2024. This work was supported in part by the Early Career Scheme (ECS) under Project 21205021 and the General Research Fund (GRF) under Project 11211122, both established under the University Grant Committee (UGC) of the Hong Kong Special Administrative Region, China; in part by the City University of Hong Kong (CityU) under Project 7020083, and Project 7006090. The associate editor coordinating the review of this article and approving it for publication was M. Xiao. *(Corresponding author: Young Jin Chun.)*

The authors are with the Department of Electrical Engineering, City University of Hong Kong, Hong Kong, China (e-mail: yunlili2-c@my.cityu.edu.hk; yjchun@cityu.edu.hk).

Color versions of one or more figures in this article are available at https://doi.org/10.1109/TWC.2024.3369662.

Digital Object Identifier 10.1109/TWC.2024.3369662

B. Related Work

Due to the growing interest in IRS technology, a considerable amount of research has been conducted in recent decades to explore design issues of IRS-aided systems. As pointed out in [8], most of them focused on link-level design. For instance, [9] considered a quasi-static phase shift design on IRS, where the mixture channel was composed of a Rayleigh faded direct link from the BS to UE and a double Rician faded IRS-assisted link. In [10], the joint design of beamformers and artificial noise at BS and phase shift matrix at the IRS was investigated for physical security. On the other hand, for IRS-aided cell-free networks, a fully decentralized cooperative beamforming design framework was proposed to increase the system sum-rate with low cost in [11].

Despite a good guidance for beamforming design of transmitter and IRS, the design work fails to perform the system-level analysis of a large-scale network. Existing studies on IRS-aided network performance have been conducted with moment matching approximated channel models, where each link followed simple fading [12], [13], [14]. For example, in [12], the first term of a Laguerre series expansion was utilized to approximate the double Rayleigh fading, and the end-to-end performance of IRS-assisted communication was compared with amplify-and-forward relay. Later, [13] considered double Nakagami-m with phase shift distribution, and derived the signal-to-noise ratio (SNR)-based performance of IRS-assisted communication in closed form by using Central Limit Theorem (CLT), while the co-channel interference was ignored. Furthermore, the system performance of IRS-assisted multi-cell networks was analyzed in [14], by approximating the double Rayleigh fading as a Complex Normal (CN) distribution through the CLT. Specifically, the interference was considered, but it was approximated by an exponential distribution and the underlying fading model was the Rayleigh distribution.

Moreover, to conduct performance analysis, extensive research has been conducted on the statistical characteristics of cascaded and mixture channels regarding relay communications, which can be categorized into two distinct groups. First, relay-assisted network has been analyzed on asymmetric cascaded channels, including mixed Rayleigh and Rician fading [15], mixed Nakagami-m and Rician fading [16], mixed $\eta-\mu$ and $\kappa-\mu$ fading channels [17]. Second, for symmetric channels, various approximation schemes have been proposed, including distribution of N generalized-K faded random variables [18], N*Nakagami distribution [19], sum distribution of non-identically squared Nakagami-m random variables [20], sum distribution of generalized Gamma random variables [21], the product of Fisher-Snedecor $\mathcal{F}$-distributed channels [22], and product distribution of κ-μ random variables [23]. In [24], the authors analyzed the dual-hop relay link with generalized fading channels by leveraging properties of advanced functions.

C. Contributions

In this paper, we address these challenges by utilizing the mixture Gamma distribution-based approximation. We introduce an accurate approximation of the fading distribution across mixed and cascaded channels of IRS-assisted wireless networks. The proposed approximation method is highly accurate, achieves tractable analysis, and is extremely versatile, which can be applied to various scenarios with majority of the known fading, such as Rayleigh, Rician, Nakagami-m, κ - μ, and κ - μ shadowed fading. We further evaluate the end-to-end performance metrics using a stochastic geometry-based framework. The main contributions of this work are summarized below.

1) We introduce a general channel modeling method for multiple types of channels in IRS-assisted networks by proving the *multiplicability* and *quadratic form* of the mixture Gamma distribution. We approximate the direct channel, cascaded channel, and mixed channel using mixture Gamma distributions with an approximation error of less than 10^{-5}. This mixture Gamma channel modeling method offers high flexibility, and works for arbitrary number of links.
2) We derive the distribution of the conditional received signal power, and the Laplace transform of the aggregated interference using stochastic geometry under two operation modes. In addition, we employ a unified analytical framework for the IRS-assisted network performance evaluation based on the proposed mixture Gamma distribution-based channel modeling method, where interested performance metrics can be expressed as functions of signal-to-interference-plus-noise ratio (SINR).
3) We present numerical simulation, which provides strong supports for the proposed channel approximation method. It is worth noting that the heavy-tailed probability density functions (PDFs) and the coherence among neighboring elements of the IRS make the moment matching-based methods inadequate for approximating the channel gain, especially for cascaded channels, even when a large-sized IRS is considered. In contrast, our proposed method of mixture Gamma approximation exhibits stable accuracy across various wireless systems, irrespective of the sample size or PDF.

D. Organizations

The remaining paper is organized as below. In Section II, we introduce the system model, association policy, and channel models. Section III introduces the necessity and sufficiency of mixture Gamma approximation for the channel modeling of individual links, and proves the multiplicability and quadratic form of mixture Gamma distributions for the channel modeling of the cascaded and mixture channels. In Section IV, we derive the channel power statistics and Laplace transform of the aggregated interference power under two operation modes and introduce a unified stochastic geometry-based system performance analysis framework for the IRS-assisted network. Simulations are provided in Section V to verify our theoretical analysis. The conclusion remarks are given in Section VI.

II. System Model

We consider an IRS-assisted multi-cell wireless network, where the IRSs are deployed to assist the downlink

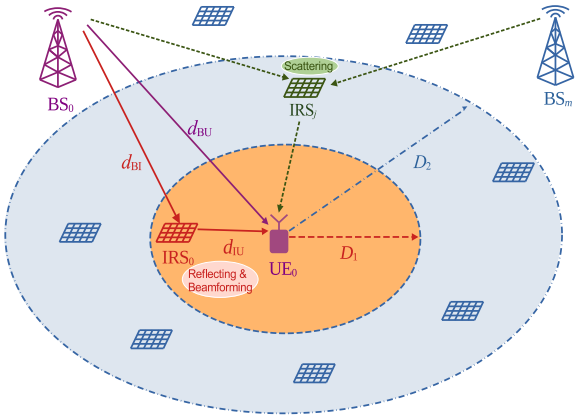

Fig. 1. Downlink of an IRS-assisted multi-cell wireless network.

transmission as shown in Fig. 1. The locations of BSs, IRSs, and UEs are modeled by independent two-dimensional (2D) homogeneous Poisson Point Processes (HPPPs), denoted as Λ_{B} with density λ_{B}, Λ_{I} with density λ_{I}, and Λ_{U} with density λ_{U}, respectively. Without loss of generality, we assume that a typical UE, denoted as UE_0, is located at the origin, and each BS has an infinitely backlogged queue. The channel is assumed to be frequency-flat and constant while the channel may vary over different frequency bands or time slots [14]. To facilitate the analysis, we employ orthogonal multiple access within each cell, implying no intra-cell interference. The common notations used in this paper are summarized in Table I.

A. BS and IRS Association Policy

We adopt a general association model for BS where each UE connects to the BS that provides strongest long-term received signal power without considering small-scale fading, denoted as BS_0, which is equivalent to connecting with the nearest BS [7]. As such, the PDF of the distance between BS_0 and UE_0, denoted as d_{BU}, could be derived from the void probability of a 2D HPPP. The PDF of d_{BU} is given by [25].

$$f_{\mathrm{d_{BU}}}(d) = 2\pi\lambda_{\mathrm{B}} d e^{-\lambda_{\mathrm{B}}\pi d^2}. \tag{1}$$

For the IRS association policy, we assume that UE_0 associates with BS_0 through at most one IRS. Additionally, when the link distances between nodes are too large, the communications suffer severe productive propagation path loss. Therefore, we define a service area for each IRS as a circle with radius D_1.[1] An interference area for each IRS is further defined, within which the IRS randomly scatters received signals to the located UEs. The radius of this interference area is denoted as D_2 [14]. Different from [14], there are no restrictions on the relationship between D_1 and D_2.

Furthermore, it has been indicated in [26], the optimal deployment location for a single associated IRS is in the vicinity of either UE_0 or BS_0. Nevertheless, as the deployment of a centralized large-scale IRS around BS_0 is usually challenging, we consider distributed deployment for IRSs and adopt the nearest association policy based on the link distance between the IRS and UE_0: If UE_0 is located within the service area of any IRS, then UE_0 associates with its nearest IRS, and the connected IRS is denoted as IRS_0.[2] Based on the distance between IRSs and UE_0, Λ_{I} is thinned into three daughter point processes:

1) The serving IRS, defined as $\Lambda_{\mathrm{I,S}} \triangleq \{\mathrm{IRS}_0 | d_{\mathrm{IU},0} \leq D_1\}$, where $d_{\mathrm{IU},0}$ represents the distance between UE_0 and its nearest IRS.
2) The interfering IRSs, defined as $\Lambda_{\mathrm{I,F}} \triangleq \{\mathrm{IRS}_j | d_{\mathrm{IU},j} \leq D_2\} \setminus \{\Lambda_{\mathrm{I,S}}\}$, where $d_{\mathrm{IU},j}$ represents the link distance of $\mathrm{IRS}_j \rightarrow \mathrm{UE}_0$, $j \in \Lambda_{\mathrm{I}}$.
3) The noising IRSs, defined as $\Lambda_{\mathrm{I,N}} \triangleq \Lambda_{\mathrm{I}} \setminus \{\Lambda_{\mathrm{I,S}} \cup \Lambda_{\mathrm{I,F}}\}$.

As such, this IRS association policy contains two operation modes:

TABLE I
COMMON NOTATIONS

Notation	Description
$\Lambda_{\mathrm{B}}, \Lambda_{\mathrm{I}}, \Lambda_{\mathrm{U}}$	Point processes of BSs, IRSs, and UEs
$\Lambda_{\mathrm{I,S}}, \Lambda_{\mathrm{I,F}}, \Lambda_{\mathrm{I,N}}$	Daughter point processes of Λ_{I}, representing the serving IRS, interfering IRSs, and noising IRSs
N	The number of reflecting elements on each IRS
D_1, D_2	The radius of IRS service area and interference area
d_{BU}, d_{BI}, d_{IU}	The distance of BS→UE, BS→IRS, and IRS→UE links
h_{BU}, $\mathbf{h}_{\mathrm{BI}}$, $\mathbf{h}_{\mathrm{IU}}^H$	The channel of BS→UE, BS→IRS, and IRS→UE links
g_{BU}, $\mathbf{g}_{\mathrm{BI}}$, $\mathbf{g}_{\mathrm{IU}}^H$	Small-scale fading channel of BS→UE, BS→IRS, and IRS→UE links
$\zeta_{\mathrm{BU}}, \zeta_{\mathrm{BI}}, \zeta_{\mathrm{IU}}$	Path loss of BS→UE, BS→IRS, and IRS→UE links
ϵ	The reference channel power gain at a distance of 1 m
$H_{\mathrm{BU}}, H_{\mathrm{BIU}}, H_{\mathrm{S}}$	Channel gain of direct path, cascaded path, and mixture channel
M_1, M_2, I	The truncation limit of mixture Gamma approximation
$(\varepsilon_i, \beta_i, \xi_i)$	Parameter tuple of mixture Gamma distributions
ω_i	The i-th weight factor of the i-th Gamma term
$f_i(x)$	PDF of the i-th Gamma component
$\underline{\mathrm{m}}$, q	The indexes of expressions for multiplicability and quadratic form of mixture Gamma distributions
m_{BU}, m_{BI}, m_{IU}	The fading parameters of BS→UE, BS→IRS, and IRS→UE links for Nakagami-m channels
S	The received signal power
$\mathrm{I_F}$	The aggregated interference power
$K_v(y)$	Modified Bessel function of the second kind
$G_{m,n}^{p,q}(y\|a,b)$	Meijer's G function
$L_p(t)$	Laguerre polynomial
t_i	The i-th zero of Laguerre polynomials
ϖ_i	The i-th weight factor of Laguerre polynomials
$\gamma(\cdot,\cdot)$	The lower incomplete Gamma function
$\Gamma(\cdot)$	The Gamma function

[1] In light of the extended transmission distance, the channel enhancement over phase alignment is considered insignificant and cannot offset the considerable productive path loss when the link distance of IRS→UE exceeds D_1. Moreover, the value of D_1 can be pragmatically determined to ensure that each IRS caters to a finite number of UEs within its immediate vicinity [14].

[2] The centralized large-scale IRS should be deployed in close proximity to the BS to serve more UEs, yet how to find a suitable location for such an IRS is usually challenging. In contrast, distributed IRSs feature smaller surface areas and offer higher flexibility in terms of positioning near either BS or UE [8]. Additionally, the performance exhibits symmetry whether the IRS is deployed in the vicinity of the BS or UE.

- **Mode 1.** If $\Lambda_{\mathrm{I,S}}$ is not empty, i.e., $d_{\mathrm{IU},0} \leq D_1$, UE_0 associates to its nearest IRS.
- **Mode 2.** If $\Lambda_{\mathrm{I,S}}$ is empty, i.e., $d_{\mathrm{IU},0} > D_1$, UE_0 does not establish a connection with any IRS.

In both **Mode 1** and **Mode 2**, if UE_0 is located within the interference areas of any IRS, it receives randomly scattered signals from the interfering IRSs, thus contributing to the interference. Otherwise, if $d_{\mathrm{IU},0} > D_2$, the effects of scattering from all IRSs can be ignored or approximated as Additive White Gaussian Noise (AWGN).

As illustrated in Fig. 1, for **Mode 1**, if there is one IRS associated with UE_0, there are two types of links between UE_0 and BS_0, including the direct link, i.e., $\mathrm{BS}_0 \rightarrow \mathrm{UE}_0$, and the cascaded link, i.e., $\mathrm{BS}_0 \rightarrow \mathrm{IRS}_0 \rightarrow \mathrm{UE}_0$. According to the void probability of the 2D HPPP, the PDF of the inter-node distance across IRS_0 and UE_0, denoted as d_{IU}, is given by [25]

$$f_{\mathrm{d_{IU}}}(d) = 2\pi\lambda_{\mathrm{I}} d e^{-\lambda_{\mathrm{I}}\pi d^2}. \tag{2}$$

To ensure tractability of the analysis, similar to [14], we assume that the distance from BS_0 to IRS_j is identical with that from BS_0 to UE_0, i.e., $d_{\mathrm{BI},j} \approx d_{\mathrm{BU}}$, where $d_{\mathrm{BI},j}$ denotes the distance between BS_0 and $\mathrm{IRS}_j, j \in \Lambda_{\mathrm{I}}$.

B. Channel Model

Assume that all BSs and UEs are equipped with a single antenna, and each IRS consists of N reflecting elements. Let $h_{\mathrm{BU}} = \sqrt{\zeta_{\mathrm{BU}}} g_{\mathrm{BU}}$ represent the channel from BS to UE, where $\zeta_{\mathrm{BU}} \triangleq \epsilon d_{\mathrm{BU}}^{-\alpha_{\mathrm{BU}}}$ indicates the BS→UE link path loss with ϵ representing the reference channel power gain at a distance of 1 m, d_{BU} denoting the BS→UE link distance, and α_{BU} being the corresponding path loss exponent. Moreover, g_{BU} represents the small-scale fading channel. Similarly, the BS→IRS and IRS→UE channels, denoted as $\mathbf{h}_{\mathrm{BI}} \in \mathbb{C}^{N\times 1}$ and $\mathbf{h}_{\mathrm{IU}}^H \in \mathbb{C}^{1\times N}$, respectively, can be modeled as

$$\mathbf{h}_{\mathrm{BI}} = \sqrt{\zeta_{\mathrm{BI}}}\mathbf{g}_{\mathrm{BI}}, \quad \mathbf{h}_{\mathrm{IU}}^H = \sqrt{\zeta_{\mathrm{IU}}}\mathbf{g}_{\mathrm{IU}}^H, \tag{3}$$

where $\zeta_{\mathrm{BI}} \triangleq \epsilon d_{\mathrm{BI}}^{-\alpha_{\mathrm{BI}}}$ and $\zeta_{\mathrm{IU}} \triangleq \epsilon d_{\mathrm{IU}}^{-\alpha_{\mathrm{IU}}}$ represent the BS→IRS and IRS→UE link path loss, respectively, with d_{BI} (d_{IU}) being the link distance and $\alpha_{\mathrm{BI}}(\alpha_{\mathrm{IU}})$ being the path loss exponent.[3] Moreover, $\mathbf{g}_{\mathrm{BI}}$ ($\mathbf{g}_{\mathrm{IU}}^H$) indicates the corresponding small-scale fading channel, respectively.

For the passive IRS, let $\mathbf{\Phi} \triangleq \mathrm{diag}(e^{j\phi_1}, \cdots, e^{j\phi_N}) \in \mathbb{C}^{N\times N}$ denote the reflection matrix, where ϕ_n is the phase shift at each element $n \in \mathcal{N} \triangleq \{1, \cdots, N\}$. Then, the cascaded BS→IRS→UE channel is given by[4]

$$\mathbf{h}_{\mathrm{BIU}} = \mathbf{h}_{\mathrm{IU}}^H \mathbf{\Phi} \mathbf{h}_{\mathrm{BI}}. \tag{4}$$

For the connected IRS_0, its phase shift is adjusted to align with the direct link based on the full CSI obtained, which is given by [8]

$$\phi_n^* = \mathrm{mod}[\angle h_{\mathrm{BU}} - (\angle[\mathbf{h}_{\mathrm{IU}}^H]_n + \angle[\mathbf{h}_{\mathrm{BI}}]_n), 2\pi], \forall n. \tag{5}$$

However, for the interfering IRSs, phase shift is not specifically designed.

The received SINR is defined as

$$\mathrm{SINR} = \frac{\mathrm{S}}{\mathrm{I_F} + \delta^2}, \tag{6}$$

where $\mathrm{S}, \mathrm{I_F}, \delta^2$ represent the received signal power, aggregated interference power, and noise power, respectively. For the given network model, the received signal at UE_0, denoted as y, can be generated in four different forms. First, when $\Lambda_{\mathrm{I,S}}$ and $\Lambda_{\mathrm{I,F}}$ are empty, the received signal and interference only come from the direct links, and we denote this case as $y^{(1)}$. Second, when $\Lambda_{\mathrm{I,S}}$ is empty and $\Lambda_{\mathrm{I,F}}$ is not empty, the received signal comes from the direct link with interference from both direct links and $\Lambda_{\mathrm{I,F}}$, and we denote this case as $y^{(2)}$. Third, when both $\Lambda_{\mathrm{I,S}}$ and $\Lambda_{\mathrm{I,F}}$ are not empty, the received signal comes from both the direct link and IRS_0-aided link with interference from both direct links and $\Lambda_{\mathrm{I,F}}$, and we denote this case as $y^{(3)}$. Fourth, when all the direct links are blocked, the signal can only be transmitted to UE_0 through IRS_0 with interference from $\Lambda_{\mathrm{I,F}}$, and we denote this case as $y^{(4)}$.

For the above four cases, we summarize the received signal envelope for each case together with the corresponding signal power S and interference power $\mathrm{I_F}$ as follows:

$$\begin{aligned} y^{(1)} &= h_{\mathrm{BU}}^{(0)} x + \sum_{m\in\Lambda_B\setminus\{0\}} h_{\mathrm{BU}}^{(m)} x' + n_0, \\ \Rightarrow \quad \mathrm{S} &= \left|h_{\mathrm{BU}}^{(0)}\right|^2, \ \mathrm{I_F} = \sum_{m\in\Lambda_B\setminus\{0\}} \left|h_{\mathrm{BU}}^{(m)}\right|^2, \end{aligned} \tag{7a}$$

$$\begin{aligned} y^{(2)} &= h_{\mathrm{BU}}^{(0)} x + \sum_{m\in\Lambda_B\setminus\{0\}} \left(h_{\mathrm{BU}}^{(m)} x' + \sum_{j\in\Lambda_{\mathrm{I,F}}} \mathbf{h}_{\mathrm{BIU},j}^{(m)} x' \right) + n_0, \\ \Rightarrow \quad \mathrm{S} &= \left|h_{\mathrm{BU}}^{(0)}\right|^2, \\ \mathrm{I_F} &= \sum_{m\in\Lambda_B\setminus\{0\}} \left(\left|h_{\mathrm{BU}}^{(m)}\right|^2 + \sum_{j\in\Lambda_{\mathrm{I,F}}} \left|\mathbf{h}_{\mathrm{BIU},j}^{(m)}\right|^2 \right), \end{aligned} \tag{7b}$$

$$\begin{aligned} y^{(3)} &= (h_{\mathrm{BU}}^{(0)} + \mathbf{h}_{\mathrm{BIU},0}^{(0)}) x \\ &\quad + \sum_{m\in\Lambda_B\setminus\{0\}} \left(h_{\mathrm{BU}}^{(m)} x' + \sum_{j\in\Lambda_{\mathrm{I,F}}} \mathbf{h}_{\mathrm{BIU},j}^{(m)} x' \right) + n_0, \\ \Rightarrow \quad \mathrm{S} &= \left|h_{\mathrm{BU}}^{(0)} + \mathbf{h}_{\mathrm{BIU},0}^{(0)}\right|^2, \\ \mathrm{I_F} &= \sum_{m\in\Lambda_B\setminus\{0\}} \left(\left|h_{\mathrm{BU}}^{(m)}\right|^2 + \sum_{j\in\Lambda_{\mathrm{I,F}}} \left|\mathbf{h}_{\mathrm{BIU},j}^{(m)}\right|^2 \right), \end{aligned} \tag{7c}$$

$$\begin{aligned} y^{(4)} &= \mathbf{h}_{\mathrm{BIU},0}^{(0)} x + \sum_{m\in\Lambda_B\setminus\{0\}} \sum_{j\in\Lambda_{\mathrm{I,F}}} \mathbf{h}_{\mathrm{BIU},j}^{(m)} x' + n_0, \\ \Rightarrow \quad \mathrm{S} &= \left|\mathbf{h}_{\mathrm{BIU},0}^{(0)}\right|^2, \ \mathrm{I_F} = \sum_{m\in\Lambda_B\setminus\{0\}} \sum_{j\in\Lambda_{\mathrm{I,F}}} \left|\mathbf{h}_{\mathrm{BIU},j}^{(m)}\right|^2, \end{aligned} \tag{7d}$$

[3]For ease of notation, we simply use α to represent the path loss exponent in the sequel for each individual link without causing confusion.

[4]Unlike conventional wireless networks, where the transmission system design can only adapt to the dynamic propagation environment without controllability, IRS offers a novel and efficient approach to combat the channel impairments between different transmission paths [27]. Note that the channel for IRS-aided communication is a mixture of the direct link (without IRS) and the cascaded link aided by IRS [28], [29].

where x is the transmitted signal with unit transmit power P_{T}, x' is the interference signal, n_0 is the received noise with power δ^2, $h_{\mathrm{BU}}^{(m)}$ is the channel of $\mathrm{BS}_m \to \mathrm{UE}_0$, $\mathbf{h}_{\mathrm{BIU},j}^{(m)}$ is the channel of $\mathrm{BS}_m \to \mathrm{IRS}_j \to \mathrm{UE}_0$, and its amplitude is given by $\left|\mathbf{h}_{\mathrm{BIU},j}^{(m)}\right| = \sum_{n=1}^{N} |h_{\mathrm{IU},j,n}^{(m)}||h_{\mathrm{BI},j,n}^{(m)}|$.

III. Mixture Gamma Approximation of Fading Channels

As we have mentioned in Section I-B, the current studies on modeling cascaded and mixture channels primarily rely on advanced functions or moment matching methods, which involve a tradeoff between accuracy and tractability. Therefore, to model the cascaded channel $\mathrm{BS}_0 \to \mathrm{IRS}_0 \to \mathrm{UE}_0$ and combined channel of the direct link $\mathrm{BS}_0 \to \mathrm{UE}_0$ and cascaded link, in this section, we derive two important properties of mixture Gamma distribution. Before that, let us first give a review of existing results on mixture Gamma distribution-based approximation.

A. Summary of Mixture Gamma Approximation

1) Necessity: In [30], it was proved that an arbitrary function $f(x)$ with a positive domain $x \in (0, \infty)$ and $\lim_{x\to+\infty} f(x) \to 0$, can be accurately approximated as a weighted sum of Gamma distributions as written in (8). Given that $f(x)$ is a valid PDF, we refer to (8) as the mixture Gamma distribution with parameter tuple $(\varepsilon_i, \beta_i, \xi_i)$, denoted as $f(x) \sim \mathcal{MG}(\varepsilon_i, \beta_i, \xi_i)$, and

$$\begin{aligned} f(x) &= \sum_{i=1}^{\infty} \omega_i f_i(x) = \sum_{i=1}^{\infty} \varepsilon_i x^{\beta_i - 1} e^{-\xi_i x} \\ &\simeq \sum_{i=1}^{I} \varepsilon_i x^{\beta_i - 1} e^{-\xi_i x}, \end{aligned} \tag{8}$$

where $f_i(x) = \frac{\xi_i^{\beta_i} x^{\beta_i - 1} e^{-\xi_i x}}{\Gamma(\beta_i)}$ is the PDF of a Gamma distribution with parameter tuple (β_i, ξ_i), $\Gamma(\cdot)$ is the Gamma function, $\omega_i = \varepsilon_i \Gamma(\beta_i) \xi_i^{-\beta_i}$ is the weight of the i-th term, I is the truncation limit that determines the approximation accuracy, and $\int_0^{\infty} f(x)\mathrm{d}x = 1$ with $f(x) \geq 0$ and $\sum_{i=1}^{\infty} \omega_i = 1$.

2) Sufficiency: In [30], the existence of a mixture Gamma function $S_u(x)$ that uniformly converges to an arbitrary function $f(x)$ was proved as written below

$$\begin{aligned} &\lim_{u\to+\infty} S_u(x) = f(x) \quad \text{uniformly for } 0 < x < \infty, \\ &\text{where } S_u(x) = \sum_{k=0}^{\infty} \frac{1}{u} f\left(\frac{k}{u}\right) \mathrm{Gamma}(k+1, u) \\ &\qquad = \sum_{k=0}^{\infty} \frac{1}{u} f\left(\frac{k}{u}\right) \cdot \frac{u^{k+1} x^k}{k!} e^{-ux}, \end{aligned} \tag{9}$$

and u is an arbitrarily large number that determines the approximation accuracy. The equality in (9) indicates that an arbitrary function $f(x)$ can be accurately approximated by a mixture of Gamma distributions $\mathrm{Gamma}(k+1, u)$ with parameters u, $k+1$ and weight $\frac{1}{u} f\left(\frac{k}{u}\right)$.

Note that (8) represents the necessity condition to construct an arbitrary function from a mixture of Gamma distributions, whereas (9) corresponds to the sufficiency condition that maps the weight ω_i and $f_i(x)$. We can find a direct relation between the arbitrary distribution $f(x)$ and tuple $(\varepsilon_i, \beta_i, \xi_i)$ by using (8) and (9) as described below

$$(\varepsilon_i, \beta_i, \xi_i) = \left(\frac{u^{i-1}}{\Gamma(i)} \cdot f\left(\frac{i-1}{u}\right), i, u\right). \tag{10}$$

As displayed in [31], the channel gain of a single link with majority of the known fading models can be approximated by the mixture Gamma distribution. Particularly, Rayleigh and Nakagami-m fading can be represented by a mixture Gamma distribution with a single term. For an arbitrary fading model, whose PDF can be approximated by a mixture Gamma distribution, I is no need to be larger than 20 with approximation error less than 10^{-5} [31].

Moreover, the statistics of mixture Gamma distribution, including the CDF, moments, and Laplace transform of a mixture Gamma distributed random variable, are derived as follows:

$$\begin{aligned} F(x) &= \sum_{i=1}^{I} \varepsilon_i \xi^{-\beta_i} \gamma(\beta_i, \xi_i x), \\ \mathbb{E}\left[x^l\right] &= \sum_{i=1}^{I} \varepsilon_i \frac{\Gamma(\beta_i + l)}{\xi_i^{\beta_i + l}}, \\ \mathcal{L}(s) &= \sum_{i=1}^{I} \varepsilon_i \frac{\Gamma(\beta_i)}{(\xi_i + s)^{\beta_i}}, \end{aligned} \tag{11}$$

where $\gamma(\cdot, \cdot)$ is the lower incomplete Gamma function.

B. Properties of Mixture Gamma Distribution

The following two theorems present the distribution of multiplicability and quadratic form for the mixture Gamma distributed channels. These theorems can be applied to derive the distribution of channel gain for cascaded and mixture channels in IRS-assisted communication.

Theorem 1 (Multiplicability): The distribution of the product of two independent, mixture Gamma distributed random variables X_1 and X_2, $Y = X_1 X_2$, can be represented by a mixture Gamma distribution with parameters $\left(\varepsilon_{\underline{m}}, \beta_{\underline{m}}, \xi_{\underline{m}}\right)$ as described below

$$\begin{aligned} \textit{Given } f_{\mathrm{X}_1}(x_1) &= \sum_{m_1=1}^{M_1} \omega_{m_1} \cdot \mathrm{Gamma}(\beta_{m_1}, \xi_{m_1}) \\ \textit{and } f_{\mathrm{X}_2}(x_2) &= \sum_{m_2=1}^{M_2} \omega_{m_2} \cdot \mathrm{Gamma}(\beta_{m_2}, \xi_{m_2}), \\ Y \textit{ has } f_{\mathrm{Y}}(y) &= \sum_{\mathcal{C}_{\underline{m}}} \varepsilon_{\underline{m}} \cdot y^{\beta_{\underline{m}} - 1} \cdot e^{-y \cdot \xi_{\underline{m}}}, \end{aligned} \tag{12}$$

where the summation range $\mathcal{C}_{\underline{m}}$ and parameters are defined as

$$\begin{aligned} &\mathcal{C}_{\underline{m}} = \{1 \leq m_1 \leq M_1,\ 1 \leq m_2 \leq M_2,\ 1 \leq i \leq I\}, \\ &\beta_{\underline{m}} = \beta_{m_1}, \quad \xi_{\underline{m}} = \frac{\xi_{m_1} \xi_{m_2}}{t_i}, \end{aligned}$$

$$\varepsilon_{\underline{m}} = \left(\prod_{j=1}^{2} \frac{\omega_{m_j} \xi_{m_j}^{\beta_{m_1}}}{\Gamma\left(\beta_{m_j}\right)} \right) \cdot \varpi_i t_i^{-\beta_{m_1}+\beta_{m_2}-1}, \tag{13}$$

t_i is the i-th root of the Laguerre polynomial $L_p(t)$, and ϖ_i is the i-th weight of the Gaussian-Laguerre quadrature $\int_0^\infty e^{-t} f(t) \mathrm{d}t \approx \sum_{i=1}^{I} \varpi_i f(t_i)$ defined as $\varpi_i = \frac{t_i}{(p+1)^2 L_{p+1}(t_i)^2}$ [32].

Proof: See Appendix A. □

Specifically, given two independent Gamma distributed random variables X_1 and X_2, the product distribution of $Y = X_1 X_2$ can be further simplified by substituting $M_1 = M_2 = 1$, $\omega_{m_1} = \omega_{m_2} = 1$ in (12), as described in the following lemma.

Lemma 1: The distribution of the product of two independent Gamma distributed random variables X_1 and X_2 is given by

$$f_{\mathrm{Y}}(y) = \sum_{i=1}^{I} \varepsilon_{\underline{m}} \cdot y^{\beta_{\underline{m}}-1} \cdot e^{-y \cdot \xi_{\underline{m}}}, \tag{14}$$

where $X_1 \sim \mathrm{Gamma}\left(\beta_{m_1}, \xi_{m_1}\right)$, $X_2 \sim \mathrm{Gamma}\left(\beta_{m_2}, \xi_{m_2}\right)$, and the parameter tuple $\left(\varepsilon_{\underline{m}}, \beta_{\underline{m}}, \xi_{\underline{m}}\right)$ is defined as follows:

$$\beta_{\underline{m}} = \beta_{m_1}, \quad \xi_{\underline{m}} = \frac{\xi_{m_1}\xi_{m_2}}{t_i},$$
$$\varepsilon_{\underline{m}} = \left(\prod_{j=1}^{2} \frac{\xi_{m_j}^{\beta_{m_1}}}{\Gamma\left(\beta_{m_j}\right)} \right) \cdot \varpi_i t_i^{-\beta_{m_1}+\beta_{m_2}-1}. \tag{15}$$

Theorem 2 (Quadratic form): Given two independent, mixture Gamma distributed random variables X^2 and Y^2, the quadratic form $S = (X+Y)^2$ follows a mixture Gamma distribution with parameter tuple $\left(\varepsilon_{\underline{q}}, \beta_{\underline{q}}, \xi_{\underline{q}}\right)$

$$f_{\mathrm{S}}(s) = \sum_{\mathcal{C}_{\underline{q}}} \left(\varepsilon_{\underline{q_1}} e^{-s \cdot \xi_{\underline{q_1}}} - \varepsilon_{\underline{q_2}} e^{-s \cdot \xi_{\underline{q_2}}} \right) \cdot s^{\beta_{\underline{q}}-1},$$

where $X^2 \sim \mathcal{MG}\left(\varepsilon_i, \beta_i, \xi_i\right)$, and $Y^2 \sim \mathcal{MG}\left(\varepsilon_j, \beta_j, \xi_j\right)$, (16)

the summation range $\mathcal{C}_{\underline{q}}$ and parameters are given by

$$\mathcal{C}_{\underline{q}} = \{1 \le i \le I,\ 1 \le j \le J,\ 0 \le k_1 \le 2\beta_j - 1,$$
$$0 \le k_2 \le 2\beta_i - 1 + k_1,\ 0 \le k_3 \le \infty\}, \tag{17}$$
$$\beta_{\underline{q}} = \beta_i + \beta_j + k_3, \quad \xi_{\underline{q_1}} = \xi_j, \quad \xi_{\underline{q_2}} = \xi_i,$$
$$\varepsilon_{\underline{q_1}} = (-1)^{k_2} \chi \cdot \xi_j^{k_2+2k_3+1}, \quad \varepsilon_{\underline{q_2}} = \chi \cdot \xi_i^{k_2+2k_3+1}, \tag{18}$$

and $\chi = \frac{\varepsilon_i \varepsilon_j \binom{2\beta_j-1}{k_1} \binom{2\beta_i-1+k_1}{k_2} (-1)^{k_1} \xi_j^{2\beta_i+k_1-k_2-1} \Gamma(\frac{k_2+1}{2})}{\Gamma(\frac{k_2+1}{2}+k_3+1)(\xi_i+\xi_j)^{2\beta_i+k_1+k_3}}$.

Proof: See Appendix B. □

Although the mixture Gamma distributions in (12) and (16) involve multiple summations, it is worth noting that these functions exhibit rapid convergence, primarily due to the swift convergence of the weight terms [31]. As depicted in Fig. 2(b), we validate that the mixture Gamma distributions achieve an approximation error of less than 10^{-5} with only 17 terms.[5]

Remark 1: As the product of two independent mixture Gamma random variables follows a mixture Gamma distribution, Theorem 1 can be easily extended to the product of K independent mixture Gamma distributed random variables. We introduce a heuristic algorithm in Appendix E to evaluate the distribution of the product of K independent mixture Gamma random variables. Similarly, the distribution of the quadratic form can also be extended to K independent mixture Gamma random variables. Hence, the analytical framework derived in this work is applicable to network environments where multiple IRSs are involved in association.

Some mixture Gamma approximations of single links and cascaded links are provided in Table II for easy reference, where the notations align with [23] and [31].

C. Effect of Phase Regulation

In this work, we consider the perfect continuous phase regulation of the associated IRS to achieve a concise expression. Subsequently, we delve into the discussion about the impact of phase regulation on the proposed channel modeling method.

For the cascaded channel, the modeling of channel gain remains unaffected by imperfect phase estimation or phase shift quantization. This is because the distribution of the received signal power in the cascaded channel depends solely on the product of the amplitudes of individual links.

However, the situation is different for the mixture channel, where the imperfect alignment of phases from different transmission paths indeed affects the received signal distribution. Nevertheless, if we can model the scaling of the received signal power caused by the phase difference between the direct link and IRS-aided cascaded link as a mixture Gamma distribution, it becomes feasible to similarly model the channel gain of the mixture channel by utilizing the proved multiplicability and quadratic form for mixture Gamma distribution, which is beyond the scope of this work. Moreover, the influence of phase shift quantization can be represented as an asymptotic scaling factor, denoted as $\eta(b) = \left[\frac{2^b}{\pi} \sin\left(\frac{\pi}{2^b}\right)\right]^2$, where b represents the number of bits used for quantizing the phase shift. As a result, the influence of phase shift quantization can be incorporated into the mixture Gamma distribution of the received signal power by scaling the distribution in Theorem 2, as shown in [33].

IV. Performance Analysis

With Theorem 1 and Theorem 2 provided in the previous section, in this section, we further illustrate the channel power statistics of the channels in IRS-assisted network. Moreover, the Laplace transform of the aggregated interference is derived, and a stochastic geometry-based analysis framework is introduced to evaluate various performance metrics.

A. Channel Power Statistics

For performance analysis, we assume that the transmit power is unit, and the reflecting elements on the same IRS experience identical small-scale fading due to high coherence. Besides, the amplitude g_{BU}, $|g_{\mathrm{BI},n}|$ and $|g_{\mathrm{IU},n}|$ follow Nakagami-m distributions with parameters m_{BU}, m_{BI} and m_{IU}, respectively. Let us denote the power terms as follows:

$$H_{\mathrm{BU}} \triangleq |h_{\mathrm{BU}}|^2 = \epsilon d_{\mathrm{BU}}^{-\alpha} |g_{\mathrm{BU}}|^2, \tag{19}$$

[5]The benchmark of the Gamma distribution in MATLAB has an error of approximately 10^{-6}.

TABLE II
MIXTURE GAMMA APPROXIMATION OF CHANNEL GAIN FOR VARIOUS FADING DISTRIBUTIONS

	Parameters of Mixture Gamma Approximation for Channel Gain		
Channel Type	ε_i	β_i	ξ_i
Rayleigh	$\frac{1}{\overline{\gamma}}$	1	$\frac{1}{\overline{\gamma}}$
Double Rayleigh	$\frac{1}{\overline{\gamma_1}\overline{\gamma_2}}\varpi_i t_i^{-1}$	$\frac{1}{\overline{\gamma_1}}$	t_i^{-1}
Nakagami-m	$\frac{m^m}{\Gamma(m)}$	m	m
Double Nakagami-m	$\frac{(m_1 m_1)^{m_1}\varpi_i t_i^{m_2-m_1-1}}{\Gamma(m_1)\Gamma(m_1)}$	m_1	$\frac{m_1 m_2}{t_i}$
Rician	$\frac{1+n^2}{e^{n^2}[(i-1)!]^2\overline{\gamma}}\left(\frac{n^2(1+n^2)}{\overline{\gamma}}\right)^{i-1}$	i	$\frac{(1+n^2)}{\overline{\gamma}}$
κ-μ	$\frac{\mu^{\mu+2i-2}\kappa^{i-1}(1+\kappa)^{\mu+i-1}}{(i-1)!e^{\kappa\mu}\Gamma(\mu+i-1)\overline{\gamma}^{\mu+i-1}}$	$\mu+i-1$	$\frac{\mu(1+\kappa)}{\overline{\gamma}}$
Double κ-μ	$\frac{(\kappa_1\mu_1)^{m_1}(\kappa_2\mu_2)^{m_2}[(1+\kappa_1)(1+\kappa_2)\mu_1\mu_2]^{m_1+\mu_1}}{m_1!m_2!e^{\mu_1\kappa_1}e^{\mu_2\kappa_2}\Gamma(m_1+\mu_1)\Gamma(m_2+\mu_2)\overline{\gamma_1\gamma_2}^{m_1+\mu_1}}\cdot\varpi_i t_i^{m_2+\mu_2-m_1-\mu_1-1}$	$m_1+\mu_1$	$\frac{(1+\kappa_1)(1+\kappa_2)\mu_1\mu_2}{\overline{\gamma_1\gamma_2}t_i}$

$$H_{\mathrm{BIU}} = |\mathbf{h}_{\mathrm{BIU}}|^2 = \epsilon^2 d_{\mathrm{BI}}^{-\alpha} d_{\mathrm{IU}}^{-\alpha}\left|\sum_{n=1}^{N}|g_{\mathrm{IU},n}||g_{\mathrm{BI},n}|\right|^2, \quad (20)$$

$$H_{\mathrm{S}} \triangleq \left||h_{\mathrm{BU}}| + |\mathbf{h}_{\mathrm{BIU}}|\right|^2. \quad (21)$$

1) Single Path: As g_{BU}, $|g_{\mathrm{BI},n}|$ and $|g_{\mathrm{IU},n}|$ follow Nakagami-m distributions, the power term H_{BU} follows a Gamma distribution, whereas the statistics of H_{BIU} is characterized by the mixture Gamma distribution and the parameter tuples are described in the following lemmas.

Lemma 2: H_{BU} follows the Gamma distribution, which can be modeled as a mixture Gamma distribution with $I = 1$ and

$$(\varepsilon_{\mathrm{BU}}, \beta_{\mathrm{BU}}, \xi_{\mathrm{BU}}) = \left(\frac{(d_{\mathrm{BU}}^{\alpha} m_{\mathrm{BU}})^{m_{\mathrm{BU}}}}{\epsilon^{m_{\mathrm{BU}}}\Gamma(m_{\mathrm{BU}})}, m_{\mathrm{BU}}, \frac{m_{\mathrm{BU}} d_{\mathrm{BU}}^{\alpha}}{\epsilon}\right). \quad (22)$$

Lemma 3: By Theorem 1, H_{BIU} follows the mixture Gamma distribution as (12) with parameters given by

$$\varepsilon_{\mathrm{BIU},i} = \frac{(m_{\mathrm{BI}} m_{\mathrm{IU}})^{m_{\mathrm{BI}}}\varpi_i t_i^{m_{\mathrm{IU}}-m_{\mathrm{BI}}-1}}{\Gamma(m_{\mathrm{BI}})\Gamma(m_{\mathrm{IU}})}\left(\frac{\nu}{N^2}\right)^{m_{\mathrm{BI}}},$$
$$\beta_{\mathrm{BIU},i} = m_{\mathrm{BI}}, \quad \xi_{\mathrm{BIU},i} = \frac{m_{\mathrm{BI}} m_{\mathrm{IU}}\nu}{t_i N^2}, \quad (23)$$

where $\nu = \frac{d_{\mathrm{BI}}^{\alpha} d_{\mathrm{IU}}^{\alpha}}{\epsilon^2}$, and $I = 17$ achieves sufficient approximation error of less than 10^{-5}.

2) Mixture Path: In the following Lemma, we use Theorem 2 to characterize the distribution of the combined channel, given that the channel gain of the individual paths follows a mixture Gamma distribution.

Lemma 4: Given that the channel gain of the direct link and cascaded link follows mixture Gamma distributions, the channel gain of the combined channel, H_{S}, follows a mixture Gamma distribution as (16) with parameters given by

$$\mathcal{C}_{\boldsymbol{q}} = \{1 \le i \le I,\ j = 1, 0 \le k_1 \le 2m_{\mathrm{BU}} - 1,$$
$$0 \le k_2 \le 2m_{\mathrm{BI}} - 1 + k_1,\ 0 \le k_3 \le \infty\},$$
$$\beta_{\boldsymbol{q}} = \beta_{\mathrm{BIU},i} + \beta_{\mathrm{BU}} + k_3, \quad \xi_{\boldsymbol{q_1}} = \xi_{\mathrm{BU}}, \quad \xi_{\boldsymbol{q_2}} = \xi_{\mathrm{BIU},i},$$
$$\varepsilon_{\boldsymbol{q_1}} = (-1)^{k_2}\chi\cdot\xi_{\mathrm{BU}}^{k_2+2k_3+1}, \quad \varepsilon_{\boldsymbol{q_2}} = \chi\cdot\xi_{\mathrm{BIU},i}^{k_2+2k_3+1},$$
$$\chi = \rho\frac{\varepsilon_{\mathrm{BIU},i}\varepsilon_{\mathrm{BU}}\xi_{\mathrm{BU}}^{2\beta_{\mathrm{BIU},i}+k_1-k_2-1}}{(\xi_{\mathrm{BIU},i}+\xi_{\mathrm{BU}})^{2\beta_{\mathrm{BIU},i}+k_1+k_3}},$$

where $\rho = \frac{\binom{2\beta_{\mathrm{BU}}-1}{k_1}\binom{2\beta_{\mathrm{BIU},i}-1+k_1}{k_2}(-1)^{k_1}\Gamma(\frac{k_2+1}{2})}{\Gamma(\frac{k_2+1}{2}+k_3+1)}$.

B. Laplace Transform of the Aggregated Interference Power

It is a well-known fact that a tractable closed-form expression of the aggregated interference only exists for deterministic channel or Rayleigh fading with PPP adopted. If the considered fading is beyond Rayleigh, the aggregated interference follows a stable distribution with four parameters, namely, stability, skew, drift, and dispersion [34]. Despite the availability of closed-form distribution expressed by Fox's H functions, the analysis of system performance becomes intractable. Thus, we use the Laplace transform of the aggregated interference to characterize the distribution, which is widely adopted in stochastic geometry [7].

The interference power received at UE_0 from direct links and cascaded links can be given by $\mathrm{I}_{\mathrm{F},1}$ and $\mathrm{I}_{\mathrm{F},2}$, respectively

$$\mathrm{I}_{\mathrm{F},1} = \sum_{m\in\Lambda_{\mathrm{B}}\setminus\{0\}} H_{\mathrm{BU}}^{(m)},$$
$$\mathrm{I}_{\mathrm{F},2} = \sum_{m\in\Lambda_{\mathrm{B}}\setminus\{0\}}\sum_{j\in\Lambda_{\mathrm{I,F}}} H_{\mathrm{BIU},j}^{(m)}, \quad (24)$$

where $H_{\mathrm{BU}}^{(m)}$ is the channel gain of $\mathrm{BS}_m \to \mathrm{UE}_0$ link, and $H_{\mathrm{BIU},j}^{(m)}$ is the channel gain of $\mathrm{BS}_m \to \mathrm{IRS}_j \to \mathrm{UE}_0$ link.

Laplace transform of the aggregated interference power can be expressed as

$$\mathcal{L}_{\mathrm{I}_{\mathrm{F},1}}|_{d_{\mathrm{BU}}^{(0)}} = \mathbb{E}[e^{-s\mathrm{I}_{\mathrm{F},1}}]|_{d_{\mathrm{BU}}^{(0)}} = \mathbb{E}_{\Lambda_B\setminus\{0\}}\left\{e^{-sH_{\mathrm{BU}}}\right\}\Big|_{d_{\mathrm{BU}}^{(0)}},$$
$$\mathcal{L}_{\mathrm{I}_{\mathrm{F},2}}|_{d_{\mathrm{BU}}^{(0)},d_{\mathrm{IU},0}} = \mathbb{E}_{\Lambda_B\setminus\{0\},\Lambda_{\mathrm{I,F}}}\left\{e^{-sH_{\mathrm{BIU}}}\right\}\Big|_{d_{\mathrm{BU}}^{(0)},d_{\mathrm{IU},0}}, \quad (25)$$

where $d_{\mathrm{BU}}^{(m)}$ is the distance from BS_m to UE_0, and $d_{\mathrm{IU},j}$ is the distance from IRS_j to UE_0. The full expressions of (25) are given in (46), (49), shown at the bottom of page 14, and derived in Appendix C.

If $\Lambda_{\mathrm{I,F}}$ is empty, the aggregated interference and its corresponding Laplace transform are given by

$$\mathrm{I}_{\mathrm{F}} = \mathrm{I}_{\mathrm{F},1}, \quad \mathcal{L}_{\mathrm{I}_{\mathrm{F}}}|_{d_{\mathrm{BU}}^{(0)}} = \mathbb{E}[e^{-s\mathrm{I}_{\mathrm{F},1}}]|_{d_{\mathrm{BU}}^{(0)}} = \mathcal{L}_{\mathrm{I}_{\mathrm{F},1}}|_{d_{\mathrm{BU}}^{(0)}}. \quad (26)$$

If $\Lambda_{\mathrm{I,F}}$ is not empty, the aggregated interference and its corresponding Laplace transform are given by

$$\mathrm{I_F} = \mathrm{I_{F,1}} + \mathrm{I_{F,2}},\ \mathcal{L}_{\mathrm{I_F}}|_{d_{\mathrm{BU},0}^{(0)},d_{\mathrm{IU},0}} = \mathcal{L}_{\mathrm{I_{F,1}}}|_{d_{\mathrm{BU}}^{(0)}} \cdot \mathcal{L}_{\mathrm{I_{F,2}}}|_{d_{\mathrm{BU},0}^{(0)},d_{\mathrm{IU},0}}. \tag{27}$$

The CDF of the aggregated interference power can be numerically obtained by taking the inverse Laplace transform of $\mathcal{L}_{\mathrm{I}|_{d_{\mathrm{BU},0}^{(0)},d_{\mathrm{IU},0}}}(s)$ as

$$F_{\mathrm{I_F}|_{d_{\mathrm{BU},0}^{(0)},d_{\mathrm{IU},0}}}(x) = \mathcal{L}^{-1}\left[\frac{1}{s}\mathcal{L}_{\mathrm{I_F}|_{d_{\mathrm{BU},0}^{(0)},d_{\mathrm{IU},0}}}(s)\right](x), \tag{28}$$

and MATLAB offers software library to evaluate the operation [14].

C. Analytical Framework

We adopt an analytical framework to assess the system performance metrics by using stochastic geometry. The original idea was proposed by Hamdi in [35] for Nakagami-m fading, later in [6] for κ - μ and η - μ fading, and then in [7] for κ - μ shadowed fading. We further extend this framework to IRS-assisted networks with mixture Gamma distributed channels, where the performance metrics of interest are evaluated and represented as functions of SINR, $g(\mathrm{SINR})$, including the spectral efficiency, moments of SINR, and outage probability.

Theorem 3: For an IRS-assisted network over generalized fading, whose received signal can be modeled as a mixture Gamma distribution with parameter tuple $(\varepsilon_i, \beta_i, \xi_i)$, $\mathbb{E}[g(\mathrm{SINR})]$ *is given by*

$$\begin{aligned}\mathbb{E}[g(\mathrm{SINR})] &= \int_0^\infty g(\mathrm{SINR}) f_{\mathrm{S}}(s)\mathrm{d}s \\ &= \sum_{i=1}^{I} \varepsilon_i \Gamma(\beta_i) {\xi_i}^{-\beta_i} \int_0^\infty g_{\beta_i}(z) \frac{\mathcal{L}_{\mathrm{I_F}}(\xi_i z)}{e^{\delta^2 \xi_i z}}\mathrm{d}z,\end{aligned} \tag{29}$$

where $g_{\beta_i}(z)$ *is defined as*

$$g_{\beta_i}(z) = \frac{1}{\Gamma(\beta_i)}\frac{\mathrm{d}^{\beta_i}}{\mathrm{d}z^{\beta_i}} z^{\beta_i - 1} g(z). \tag{30}$$

Proof: See Appendix D. □

In the following, we apply Theorem 3 to evaluate several system performance metrics of interest by invoking their SINR functions.

1) Spectral Efficiency: Spectral efficiency is given by [36]

$$\mathcal{R} = \mathbb{E}[\ln(1 + \mathrm{SINR})]. \tag{31}$$

By substituting $g(z) = \ln(1+z)$ and $g_{\beta_i}(z)$ to (29) [35]

$$g_{\beta_i}(z) = \frac{1}{\Gamma(\beta_i)}\frac{\mathrm{d}^{\beta_i}}{\mathrm{d}z^{\beta_i}} z^{\beta_i - 1} g(z) = \frac{1}{z}\left(1 - \frac{1}{(1+z)^{\beta_i}}\right), \tag{32}$$

the spectral efficiency of an IRS-assisted wireless network is evaluated as follows:

$$\mathcal{R} = \sum_{i=1}^{I} \varepsilon_i \Gamma(\beta_i) {\xi_i}^{-\beta_i} \int_0^\infty \frac{1}{z}\left(1 - \frac{1}{(1+z)^{\beta_i}}\right) \frac{\mathcal{L}_{\mathrm{I_F}}(\xi_i z)}{e^{\delta^2 \xi_i z}}\mathrm{d}z. \tag{33}$$

2) Moments of SINR: The moments of the SINR $\mathbb{E}[\mathrm{SINR}^l]$ can be derived by substituting $g(z) = z^l$ and $g_{\beta_i}(z)$ to (29) [7]

$$g_{\beta_i}(z) = \frac{1}{\Gamma(\beta_i)}\frac{\mathrm{d}^{\beta_i}}{\mathrm{d}z^{\beta_i}} z^{\beta_i - 1} g(z) = \frac{\Gamma(\beta_i + l)}{\Gamma(l)\Gamma(\beta_i)} z^{l-1}. \tag{34}$$

Then, the moments of the SINR are evaluated as follows:

$$\mathbb{E}[\mathrm{SINR}^l] = \sum_{i=1}^{I} \varepsilon_i {\xi_i}^{-\beta_i} \int_0^\infty \frac{\Gamma(\beta_i + l)}{\Gamma(l) e^{\delta^2 \xi_i z}} z^{l-1} \mathcal{L}_{\mathrm{I_F}}(\xi_i z)\mathrm{d}z.$$

3) Outage Probability: The outage probability is defined as written below, which is averaged over the link distance

$$P_{\mathrm{outage}} = 1 - \mathbb{P}\{\mathrm{SINR} > \tau\} = 1 - \mathbb{P}\left(\mathrm{I_F} < \frac{\mathrm{S}}{\tau} - \delta^2\right), \tag{35}$$

for a given SINR threshold τ. By substituting (28) into (35), the outage probability can be further simplified to

$$P_{\mathrm{outage}} = 1 - \mathcal{L}^{-1}\left[\frac{1}{s}\mathcal{L}_{\mathrm{I_F}|_{d_{\mathrm{BU},0}^{(0)},d_{\mathrm{IU},0}}}(s)\right]\left(\frac{\mathrm{S}}{\tau} - \delta^2\right). \tag{36}$$

V. Numerical Results

In this section, we present numerical evaluations of the theoretical results and compare them with Monte-Carlo simulations. First, we present the approximation results of both cascaded channel gain and mixture channel gain, alongside corresponding simulation results. This comparison allows us to assess the accuracy of our proposed channel approximation method. Next, by analyzing the CDF of received signal power, we gain insights into the impact of varying link distances on the received signal power. Furthermore, we investigate the influence of key parameters such as the density ratio of IRS to BS, as well as the number of reflecting elements on each IRS. Through careful analysis, we explore how these parameters affect the overall system performance. Finally, we present the system performance under different parameter setups, offering a comprehensive understanding of the system's behavior.

To better understand the mixture propagation environments and system-level performance, the numerical analysis is carried out with Nakagami-m fading. All of the simulations are conducted using MATLAB with the following parameters: the radius of the whole area is $R = 1000\,\mathrm{m}$, BS density is $\lambda_{\mathrm{B}} = 1 \times 10^{-5}/\mathrm{m}^2$, IRS density is $\lambda_{\mathrm{I}} = 1 \times 10^{-4}/\mathrm{m}^2$, the radius of service area for IRS is $D_1 = 25\,\mathrm{m}$, the radius of interference area for IRS is $D_2 = 50\,\mathrm{m}$, the transmit power of BS is $P_{\mathrm{T}} = 1\,\mathrm{Watt}$, the noise power is $\delta^2 = -90$ dBm, the number of elements on each IRS is $N = 500$, the small-scale fading parameters are $m_{\mathrm{BU}} = 2$, $m_{\mathrm{BI}} = 5$, $m_{\mathrm{IU}} = 6$, the path loss exponents are given by $\alpha_{\mathrm{BU}} = 4$, $\alpha_{\mathrm{BI}} = 3$, $\alpha_{\mathrm{IU}} = 3$, and the sample size used for the simulations is 10^6, if not specified otherwise [7], [14].

A. Channel Modeling of the Small-Scale Channel Gain

Figs. 2(a)-2(b) compare the approximated PDFs using mixture Gamma approximation, and moment matching, i.e., CLT

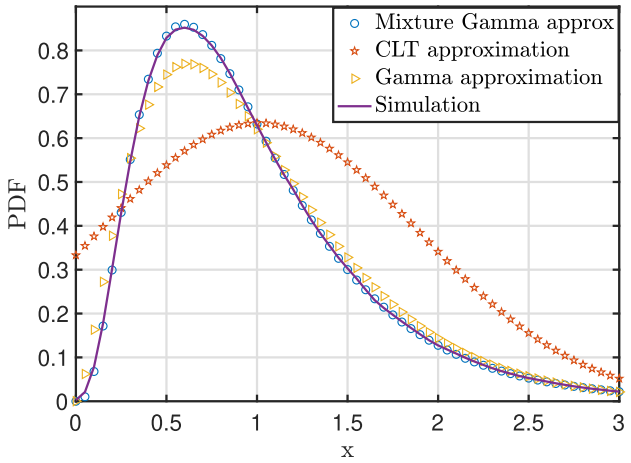

(a) PDF of the small-scale channel gain for the cascaded link.

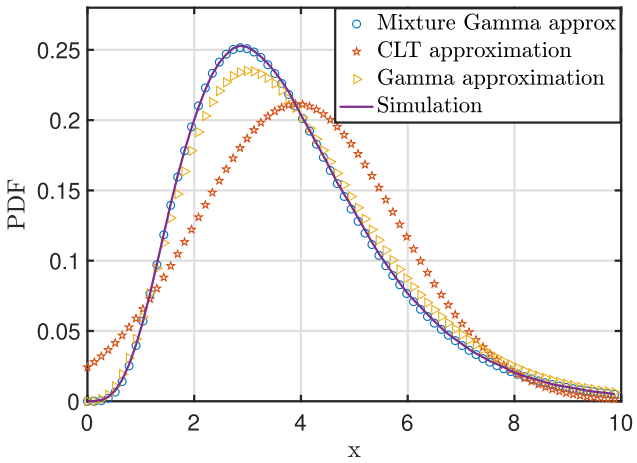

(b) PDF of the small-scale channel gain for the mixture channel.

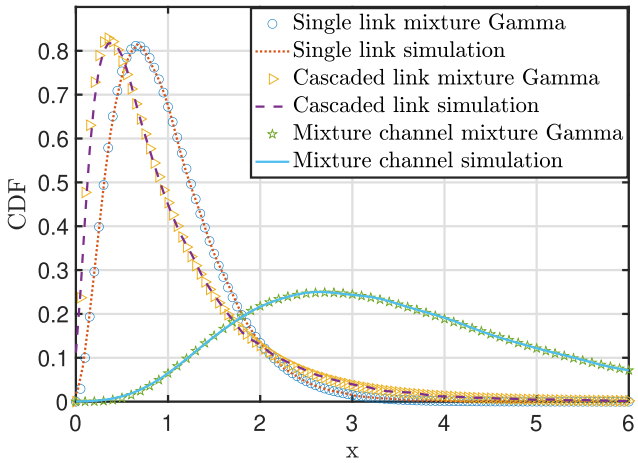

(c) PDF of the small-scale channel gain for all types of channels.

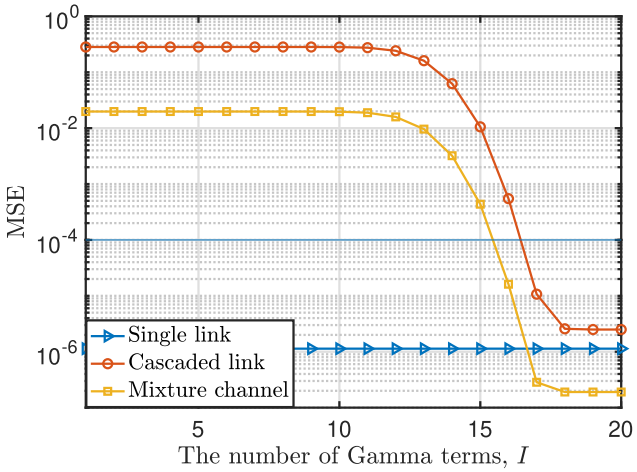

(d) MSE of mixture Gamma approximation.

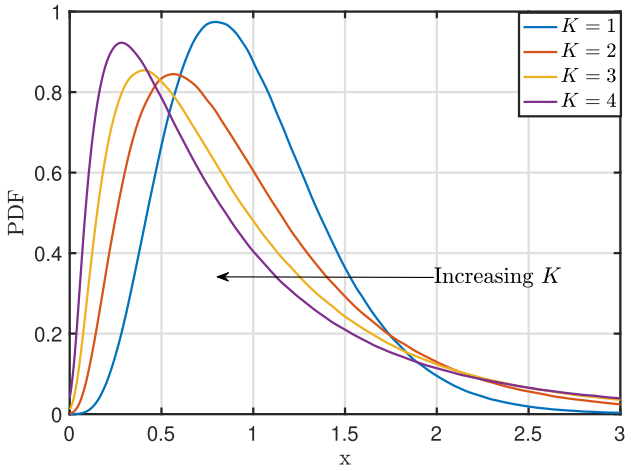

(e) PDF of the small-scale channel gain for the K-cascaded channel.

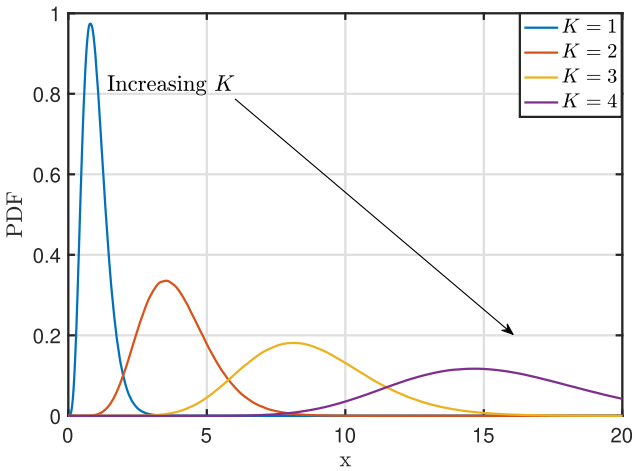

(f) PDF of the small-scale channel gain for the K-mixture channel.

Fig. 2. Channel modeling of the small-scale channel gain.

and Gamma approximation, with the simulated PDFs of the cascaded channel and mixture channel, respectively. The sample size for moment matching methods is 1000. It is observed that the mixture Gamma approximation provides a better fit to the PDFs of both channels compared to the moment matching-based approximation. This observation validates the correctness and necessity of Theorem 1 and Theorem 2. These results are expected since the accuracy of CLT approximation

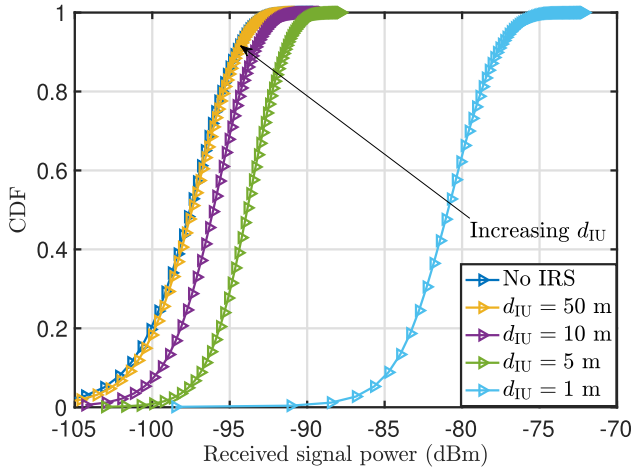

(a) CDF of the signal power with various link distances for IRS→UE.

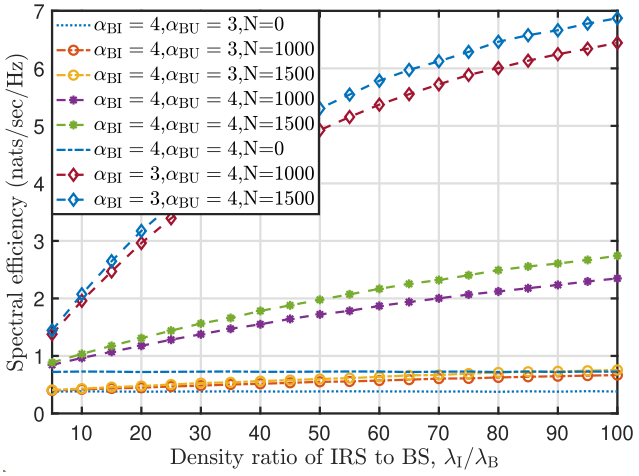

(b) Spectral Efficiency with $D_1 = 25$ m and $D_2 = 50$ m.

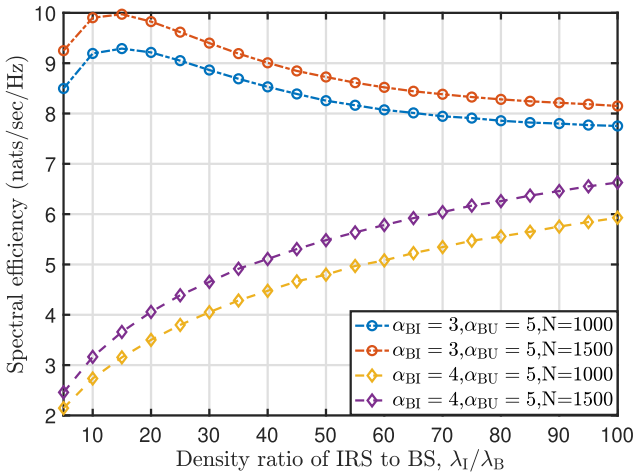

(c) Spectral Efficiency with $D_1 = R$ and $D_2 = 50$ m.

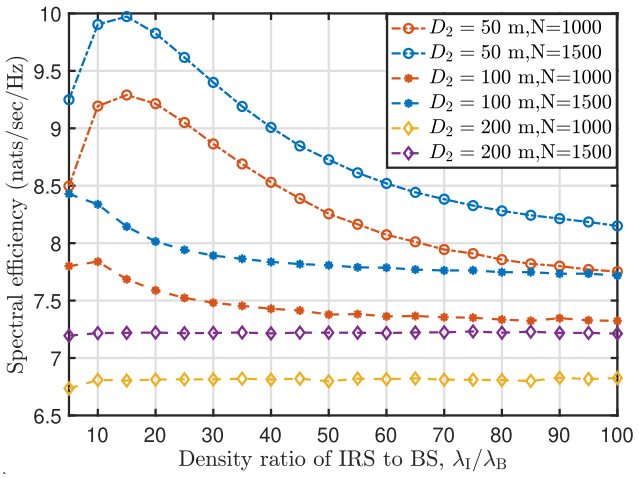

(d) Spectral Efficiency with different D_2 ($D_1 = R$, $\alpha_{\mathrm{BI}} = 3$, $\alpha_{\mathrm{BU}} = 5$).

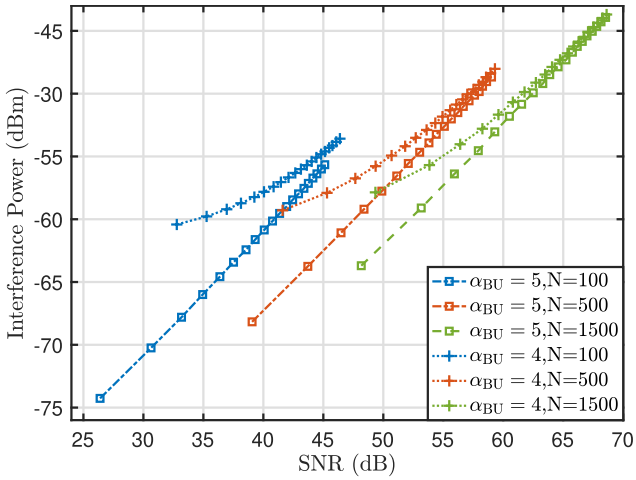

(e) Interference power versus SNR ($D_1 = D_2 = R$).

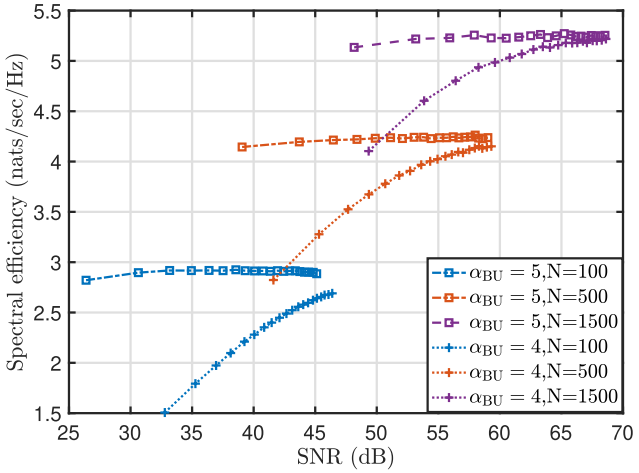

(f) Spectral efficiency versus SNR ($D_1 = D_2 = R$).

Fig. 3. System performance analysis.

relies on the tails of the PDF due to the perfect symmetry assumption of the Gaussian distribution. In the presence of a symmetric PDF, increasing the sample size can enhance the accuracy of the CLT approximation. However, for an asymmetric PDF, such an increase in sample size does not necessarily lead to improved accuracy. On the other hand,

although the Gamma distribution's PDF is asymmetric, the characteristics of the tails and peaks of the PDF for the channel gain cannot be fully captured with only the first two moments.

As presented in [37], a multiplicative process necessarily results in heavy-tailed distributions, regardless of input. Therefore, the channel coherence among neighboring elements of IRS, leading to heavy-tailed PDF for the channel gain of cascaded channel, render the light-tailed distributions, i.e., Gaussian or Exponential distributions, unsuitable to achieve accurate approximations, even in the presence of a large-sized IRS.

Then, in Fig. 2(c), the PDF of channel gain for various types of channels is displayed, i.e., single channel gain, cascaded channel gain and mixture channel gain. We can observe that the cascaded channel gain has a heavier tail compared to the single link, while the PDF of mixture channel gain has a lighter tail. These results imply that the cascaded channel can exhibit extreme outcomes more frequently, whereas the mixture channel averages over both paths.

Next, Fig. 2(d) showcases the mean square error (MSE) of the mixture Gamma approximation between two PDFs applied to various types of channels. The first PDF is obtained experimentally from 10^7 samples, while the second PDF is derived from the mixture Gamma distribution. These results corroborate that for multiple channel types with Nakagami-m fading, the approximation error remains below 10^{-5} when the number of Gamma components in the mixture Gamma distribution exceeds 17. Notably, the simulation error of 10^{-6} observed in the single channel is attributed to the MATLAB program. This is because the PDF of the channel gain for the channel experiencing Nakagami-m fading precisely follows a mixture Gamma distribution with $I = 1$, without requiring any approximation.

Furthermore, Figs. 2(e)-2(f) depict the PDFs of the K-cascaded channel and K-mixture channel, respectively. Two noteworthy observations arise from these figures: First, as the value of K increases, the PDF of the cascaded channel exhibits a heavier tail. Second, as the value of K increases, the tail of the PDF for the mixture channel becomes lighter. These findings align with the theoretical analysis on multiplicative and additive processes presented in [37].

B. System Performance Analysis

In Fig. 3(a), we display the CDF of the received signal power based on varying link distance between the typical UE and its serving IRS, d_{IU}. These results show that the benefit of decreasing d_{IU} is more pronounced when d_{IU} is smaller. This phenomenon can be attributed to the presence of product-distance path loss of the cascaded link assisted by IRS, which becomes more significant at larger distances. These observations align with results reported in [14].

Fig. 3(b) presents the spectral efficiency versus the density ratio of IRS to BS, $\lambda_{\mathrm{I}}/\lambda_{\mathrm{B}}$, considering different numbers of reflecting elements on each IRS, N, and different path loss exponents, where $D_1 = 25$ m, $D_2 = 50$ m, and $\alpha_{\mathrm{BI}} = \alpha_{\mathrm{IU}}$. It is observed that the performance enhancement facilitated by IRS is affected by the disparity in channel conditions between the direct link and the cascaded channel. When the path loss exponent of the cascaded link is larger than that of the direct link, i.e., $\alpha_{\mathrm{BI}} > \alpha_{\mathrm{BU}}$, the performance improvement provided by IRS is limited. In contrast, when path loss exponent of the cascaded link is smaller than the direct link, i.e., $\alpha_{\mathrm{BI}} < \alpha_{\mathrm{BU}}$, the system can achieve equivalent spectral efficiency with only a fraction (approximately one-tenth) of the required IRSs compared to the scenario where $\alpha_{\mathrm{BU}} = \alpha_{\mathrm{BI}}$. Additionally, the curves exhibit identical shapes when employing the same D_1 and D_2 settings as in [14]. The selection of appropriate D_1 and D_2 values can be determined according to practical scenarios that involve different blockage models.

Subsequently, we study the impact of different D_1 and D_2 settings in Figs. 3(c)-3(d). D_1 represents the maximum distance between the typical UE and its associated IRS and it is set as $D_1 = R$, which means the link distance between the typical UE and its serving IRS is not restricted in the simulation. In contrast, we set smaller maximum connection distance for the interfering IRSs compared to the serving IRS, considering that the received signal power through IRS-assisted channel benefits from the power gain with an order of $O(N^2)$, while that of the interfering IRSs is $O(N)$. Due to the larger power gain offered by the associated IRS, the transmitted signal may persist more chance to propagate farther than interference signals.

As shown in Fig. 3(c), the spectral efficiency under different path loss exponents behaves differently with $D_2 = 50$ m, where the direct link suffers severe path loss, i.e., $\alpha_{\mathrm{BU}} = 5$. It is observed that when $\alpha_{\mathrm{BI}} = 3$, the spectral efficiency initially increases and then decreases with the increasing density ratio. On the other hand, the spectral efficiency keeps increasing with the density ratio when $\alpha_{\mathrm{BI}} = 4$. Intuitively, in a scenario where the interference area is small, i.e., $D_2 = 50$ m, there is an optimal IRS density due to the tradeoff between signal power and interference power, when the channel conditions differ significantly between the direct link and the cascaded link, i.e., $\alpha_{\mathrm{BI}} = 3$, $\alpha_{\mathrm{BU}} = 5$. However, when the difference of the channel condition between the direct link and cascaded link is small, i.e., $\alpha_{\mathrm{BI}} = 4$ while $\alpha_{\mathrm{BU}} = 5$, the advantage of the performance gain provided by IRS at the low IRS density disappears.

In Fig. 3(d), the spectral efficiency is plotted against the density ratio of IRS to BS with different D_2, where $\alpha_{\mathrm{BI}} = 3$ and $\alpha_{\mathrm{BU}} = 5$. As D_2 increases, indicating an increase in the number of interfering IRSs, the spectral efficiency decreases. Moreover, for large values of D_2, such as $D_2 = 100$ m or $D_2 = 200$ m, the spectral efficiency reaches a saturation point, as the density ratio of IRS to BS increases within the given setup, where the channel condition of the cascaded link is much better than that of the direct link. This phenomenon is reasonable as the received signal power is dominated by the IRS-assisted cascaded link, which is enhanced due to a shorter connection distance between the typical UE and its serving IRS. Meanwhile, the interference power is also strengthened due to the shorter link distances and the presence of more interfering IRSs. As a consequence, in scenarios characterized

by a weak direct link, the performance becomes limited by interference when there is a high density ratio of IRS to BS.

In order to gain deeper insights into the saturation phenomenon arising from a high IRS density, we illustrate the interference power and spectral efficiency versus the SNR with $D_1 = D_2 = R$ in Figs. 3(e)-3(f), where the transmission of both signal and interference is not limited by link distance. It is observed that as the density ratio of IRS to BS increases and the direct link suffers severe path loss, i.e., $\alpha_{\mathrm{BU}} = 5$, the interference power exhibits a linear growth pattern alongside the signal power. Consequently, despite having a higher SNR, the spectral efficiency reaches a saturation point at high density ratios of IRS to BS. On the other hand, when the channel condition of the direct link is acceptable, i.e., $\alpha_{\mathrm{BU}} = 4$, the saturation of spectral efficiency diminishes due to the contribution of the direct link to both signal power and interference power.

VI. Conclusion

We have developed a comprehensive analytical framework for system performance in IRS-assisted multi-cell wireless networks, which has been achieved through the introduction of a novel statistical channel modeling method based on the mixture Gamma distribution. We first modeled the channel gain of cascaded and mixed channels as mixture Gamma distributions by proving its multiplicability and quadratic form. These two properties allow us to model a wide range of channel types, regardless of the fading characteristics of individual links or the number of links involved. Then, we evaluated the distribution of the received signal power and the Laplace transform of the aggregated interference for two operation modes. Furthermore, the analytical framework, based on the proposed mixture Gamma channel modeling method, enables the derivation of key performance metrics such as spectral efficiency, SINR moments, and outage probability using their corresponding SINR functions. To verify the theoretical analysis, we provided numerical and simulation results. It is noteworthy that our proposed mixture Gamma distribution-based channel approximation method offers high tractability and accuracy for various types of channels, thus facilitating system analysis. We also observed that as the value of K increases, the tail of the PDF for K-cascaded channels becomes heavier, indicating a higher likelihood of extreme outcomes. Conversely, for K-mixture channels, the tail of the PDF becomes lighter with an increasing value of K.

Appendix A

In this appendix, we provide a proof for Theorem 1. It is known that the PDF of the product of two random variables whose PDFs are linear combinations of Gamma distributions could be expressed by the Meijer's G function [21], [23], [38]. Thus, we express the PDF of Y as shown in the step (a) in (37), shown at the bottom of the next page. However, such expressions with Meijer's G function will lead to mathematically intractable for the system performance analysis. To this end, by employing $G_{0,2}^{2,0}(y|b,c) = 2y^{\frac{1}{2}(b+c)}K_{b-c}(2\sqrt{y})$ in step (b), the PDF of Y is simplified to an expression with the modified Bessel function. Then, the modified Bessel function $K_v(y)$ can be further derived in (38), shown at the bottom of the next page, where $I(t)$ can be derived as

$$I(t) = \int_0^\infty e^{-t} g(t) \mathrm{d}t, \tag{39}$$

and $g(t)$ is given by:

$$g(t) = \exp\left(-\frac{y\xi_{m_1}\xi_{m_2}}{t}\right) t^{-\beta_{m_1}+\beta_{m_2}-1}. \tag{40}$$

Next, the modified Bessel function is approximated by Gaussian-Hermite functions with $\int_0^\infty e^{-t}g(t)\,dt \approx \sum_{i=0}^{I} \varpi_i g(t_i)$, which solves this integration tractably [39]. As such, the PDF of Y is achieved in (41), shown at the bottom of the next page, with the restriction that absolute phase value of y is no large than $\frac{1}{4}\pi$. Finally, with some mathematical simplifications, the PDF of the product of two mixture Gamma distributed random variables can be simplified as a mixture Gamma distribution as shown in (12). This completes the proof.

Appendix B

In this appendix, we provide a proof for Theorem 2. If X^2 follows mixture Gamma distribution, the PDF of X is given by

$$f_{\mathrm{X}}(x) = 2\sum_{i=1}^{I} \varepsilon_i x^{2\beta_i - 1} e^{-\xi_i x^2}. \tag{42}$$

Then, the PDF of $Z = X + Y$ can be derived through convolution, as shown in (43), shown at the bottom of the next page. With some simple mathematical simplifications, the step (a) in (43), is achieved by invoking $(a+x)^n = \sum_{k=0}^{n}\binom{n}{k}x^k a^{n-k}$, where $g'(x)$ can be further derived with a substitution of $t = \left(x - \frac{\xi_j}{\xi_i+\xi_j}z\right)^2$ and [40, eq.(3.381.2)], in (44), shown at the bottom of the next page. Next, by substituting (44) into (43), the PDF of Z is derived (45), shown at the bottom of the next page, where the power series expansion of incomplete Gamma function is applied in step (a). Last, the scaling properties of PDF, $f_{\mathrm{S}}(s) = \frac{1}{2}s^{-\frac{1}{2}}f_{\mathrm{Z}}(\sqrt{s})$ is utilized to derive the PDF of S. This completes the proof.

Appendix C

This appendix provides derivation of $\mathcal{L}_{\mathrm{I_{F,1}}|_{d_{\mathrm{BU}}^{(0)}}}$ and $\mathcal{L}_{\mathrm{I_{F,2}}|_{d_{\mathrm{BU}}^{(0)},d_{\mathrm{IU},0}}}$. The Laplace transform of the first component of the interference, $\mathrm{I_{F,1}}$, is derived in (46) [7], where $G_{\mathrm{BU}} = g_{\mathrm{BU}}^2$, and we apply a change of variable, i.e., $t = s\epsilon G_{\mathrm{BU}} {d_{\mathrm{BU}}}^{-\alpha}$ in step (a), then use integration by parts in step (b), and the last step is obtained with some mathematical simplifications ($\alpha \geq 2$). The first part of the expectation term in (46), $\mathbb{E}_{\mathrm{H}}\left[(s\epsilon G_{\mathrm{BU}})^{\frac{2}{\alpha}}\gamma\left(1-\frac{2}{\alpha}, s\epsilon G_{\mathrm{BU}}\left[d_{\mathrm{BU}}^{(0)}\right]^{-\alpha}\right)\right]$,

is evaluated by in (47), shown at the bottom of the next page, with the assistance of the power series expansion of lower incomplete Gamma function and the definition of Gamma function, where $d_0 = d_{\mathrm{BU}}^{(0)}$. The second part of the expectation

$$f_{\mathrm{Y}}(y) \overset{(a)}{=} \sum_{m_1=1}^{M_1}\sum_{m_2=1}^{M_2} \omega_{m_1}\omega_{m_2}\frac{\xi_{m_1}\xi_{m_2}}{\Gamma(\beta_{m_1})\Gamma(\beta_{m_2})} G_{0,2}^{2,0}\left(y\xi_{m_1}\xi_{m_2}|\beta_{m_1}-1,\beta_{m_2}-1\right)$$
$$\overset{(b)}{=} \sum_{m_1=1}^{M_1}\sum_{m_2=1}^{M_2} \omega_{m_1}\omega_{m_2}\frac{\xi_{m_1}\xi_{m_2}}{\Gamma(\beta_{m_1})\Gamma(\beta_{m_2})} \times 2(y\xi_{m_1}\xi_{m_2})^{\frac{1}{2}(\beta_{m_1}+\beta_{m_2})-1} \times K_{\beta_{m_1}-\beta_{m_2}}(2\sqrt{y\xi_{m_1}\xi_{m_2}}), \tag{37}$$

$$K_{\beta_{m_1}-\beta_{m_2}}(2\sqrt{y\xi_{m_1}\xi_{m_2}}) = \frac{1}{2}\left(y\xi_{m_1}\xi_{m_2}\right)^{\frac{\beta_{m_1}-\beta_{m_2}}{2}} \cdot \underbrace{\int_0^\infty \exp\left(-t-\frac{y\xi_{m_1}\xi_{m_2}}{t}\right) t^{-\beta_{m_1}+\beta_{m_2}-1}\mathrm{d}t}_{I(t)}, \tag{38}$$

$$f_{\mathrm{Y}}(y) = \sum_{m_1=0}^{M_1}\sum_{m_2=0}^{M_2} \frac{\omega_{m_1}\omega_{m_2}\xi_{m_1}\xi_{m_2}}{\Gamma(\beta_{m_1})\Gamma(\beta_{m_2})}(y\xi_{m_1}\xi_{m_2})^{\beta_{m_1}-1}\int_0^\infty \exp\left(-t-\frac{y\xi_{m_1}\xi_{m_2}}{t}\right)\frac{1}{t^{\beta_{m_1}-\beta_{m_2}+1}}\mathrm{d}t$$
$$= \sum_{i=1}^{I}\sum_{m_1=1}^{M_1}\sum_{m_2=1}^{M_2} \omega_{m_1}\omega_{m_2}\frac{(\xi_{m_1}\xi_{m_2})^{\beta_{m_1}}}{\Gamma(\beta_{m_1})\Gamma(\beta_{m_2})} t_i^{-\beta_{m_1}+\beta_{m_2}-1}\varpi_i y^{\beta_{m_1}-1}e^{-\frac{\xi_{m_1}\xi_{m_2}}{t_i}y}, \tag{41}$$

$$f_{\mathrm{Z}}(z) = \int_0^z f_{\mathrm{X}}(x)f_{\mathrm{Y}}(z-x)\mathrm{d}x = \int_0^z \left(2\sum_{i=1}^{I}\varepsilon_i x^{2\beta_i-1}e^{-\xi_i x^2}\right)\left(2\sum_{j=1}^{J}\varepsilon_j (z-x)^{2\beta_j-1}e^{-\xi_j(z-x)^2}\right)\mathrm{d}x$$
$$\overset{(a)}{=} \sum_{i=1}^{I}\sum_{j=1}^{J} 4\varepsilon_i\varepsilon_j \sum_{k_1=0}^{2\beta_j-1}\binom{2\beta_j-1}{k_1}(-1)^{k_1}z^{2\beta_j-k_1-1}e^{z^2\left(\frac{\xi_j^2}{\xi_i+\xi_j}-\xi_j\right)}\underbrace{\int_0^z x^{k_1+2\beta_i-1}e^{-(\xi_i+\xi_j)\left(x-\frac{\xi_j}{\xi_i+\xi_j}z\right)^2}\mathrm{d}x}_{g'(x)}, \tag{43}$$

$$g'(x) = \int_0^{\left(\frac{\xi_j}{\xi_i+\xi_j}z\right)^2}\left(\frac{\xi_j}{\xi_i+\xi_j}z-\sqrt{t}\right)^{k_1+2\beta_i-1}\frac{e^{-(\xi_i+\xi_j)t}}{2\sqrt{t}} + \left(\frac{\xi_j}{\xi_i+\xi_j}z+\sqrt{t}\right)^{k_1+2\beta_i-1}\frac{e^{-(\xi_i+\xi_j)t}}{2\sqrt{t}}\mathrm{d}t$$
$$= \frac{1}{2}\sum_{k_2=0}^{2\beta_i-1+k_1}\binom{2\beta_i-1+k_1}{k_2}\frac{(\xi_j z)^{2\beta_i-1+k_1-k_2}}{(\xi_i+\xi_j)^{2\beta_i+k_1-\frac{k_2+1}{2}}}\left[\gamma\left(\frac{k_2+1}{2},\frac{\xi_j^2z^2}{\xi_i+\xi_j}\right)+\gamma\left(\frac{k_2+1}{2},\frac{\xi_i^2z^2}{\xi_i+\xi_j}\right)\right]. \tag{44}$$

$$f_{\mathrm{Z}}(z) = \sum_{i=1}^{I}\sum_{j=1}^{J} 2\varepsilon_i\varepsilon_j e^{-\frac{\xi_i\xi_j}{\xi_i+\xi_j}z^2}\sum_{k_1=0}^{2\beta_j-1}\binom{2\beta_j-1}{k_1}(-1)^{k_1}\sum_{k_2=0}^{2\beta_i+k_1-1}\binom{2\beta_i+k_1-1}{k_2}z^{2\beta_i+2\beta_j-2-k_2}$$
$$\cdot\frac{\xi_j^{2\beta_i-1+k_1-k_2}}{(\xi_i+\xi_j)^{2\beta_i+k_1-\frac{k_2+1}{2}}}\left[(-1)^{k_2}\gamma\left(\frac{k_2+1}{2},\frac{\xi_j^2z^2}{\xi_i+\xi_j}\right)+\gamma\left(\frac{k_2+1}{2},\frac{\xi_i^2z^2}{\xi_i+\xi_j}\right)\right]$$
$$\overset{(a)}{=} \sum_{i=1}^{I}\sum_{j=1}^{J} 2\varepsilon_i\varepsilon_j \sum_{k_1=0}^{2\beta_j-1}\binom{2\beta_j-1}{k_1}(-1)^{k_1}\sum_{k_2=0}^{2\beta_i+k_1-1}\binom{2\beta_i+k_1-1}{k_2}\frac{\Gamma(\frac{k_2+1}{2})\xi_j^{2\beta_i-1+k_1-k_2}z^{2\beta_i+2\beta_j+2k_3-2}}{\Gamma(\frac{k_2+1}{2}+k_3+1)(\xi_i+\xi_j)^{2\beta_i+k_1+k_3}}$$
$$\cdot\left[(-1)^{k_2}\xi_j^{k_2+1+2k_3}e^{-\xi_j z^2}+\xi_i^{k_2+1+2k_3}e^{-\xi_i z^2}\right], \tag{45}$$

term is derived by directly utilizing the Laplace transform of the Gamma distribution, as shown in (48),

$$\mathbb{E}_2 = -\left[d_{\mathrm{BU}}^{(0)}\right]^2\left[1-\left(\frac{m_{\mathrm{BU}}}{s'+m_{\mathrm{BU}}}\right)^{m_{\mathrm{BU}}}\right], \tag{48}$$

where $s' = s\epsilon {d_{\mathrm{BU}}^{(0)}}^{-\alpha}$. Following a similar procedure, $\mathcal{L}_{\mathrm{I_{F,2}}|_{d_{\mathrm{BIU}}^{(0)}}}$ can be derived as shown in (49), where $G_{\mathrm{BIU}} = \left|\sum_{n=1}^{N}|g_{\mathrm{IU},n}||g_{\mathrm{BI},n}|\right|^2$, and $\eta = \epsilon^2 d_{\mathrm{IU}}^{-\alpha} G_{\mathrm{BIU}}$.

APPENDIX D

In this appendix, we provide a proof for Theorem 3. The average of an arbitrary function of the SINR, $\mathbb{E}[g(\mathrm{SINR})]$, is illustrated in (50), shown at the bottom of the page. First, the PDF of the mixture Gamma distribution is used in the second equality, then a change of variable, i.e., $z = \frac{H_{\mathrm{S}}}{\mathrm{I_F}+\delta^2}$, is applied in step (a), and a substitution of $b = \xi_i(\mathrm{I_F}+\delta^2)$ is utilized in step (b). Next, Q is evaluated in (51) by utilizing the partial integral as follows

$$Q = -\sum_{k=0}^{\beta_i-1} g_k(z) b^{\beta_i-k-1} e^{-bz}\big|_0^{\infty} + \int_0^{\infty} g_{\beta_i}(z) e^{-bz}\mathrm{d}z, \tag{51}$$

and the last equality in (50) is achieved. This completes the proof.

APPENDIX E

In this appendix, we present an iteration algorithm that enables us to obtain the PDF of mixture Gamma distribution for K-cascaded channels, as shown in Algorithm 1. Furthermore, we can use a similar iterative procedure as Algorithm 1 to straightforwardly achieve the mixture Gamma distribution PDF for the K-mixture channels.

$$\begin{aligned}
\mathcal{L}_{\mathrm{I_{F,1}}|_{d_{\mathrm{BU}}^{(0)}}} &= \exp\left(-2\pi\lambda_{\mathrm{B}}\int_{d_{\mathrm{BU}}^{(0)}}^{\infty}\left(1-\mathbb{E}_{\mathrm{H}}\left[e^{-s\epsilon G_{\mathrm{BU}} d_{\mathrm{BU}}^{-\alpha}}\right]\right) d_{\mathrm{BU}}\mathrm{d}d_{\mathrm{BU}}\right)\\
&\overset{(a)}{=} \exp\left(-2\pi\lambda_{\mathrm{B}}\mathbb{E}_{\mathrm{H}}\left[\frac{(s\epsilon G_{\mathrm{BU}})^{\frac{2}{\alpha}}}{\alpha}\int_0^{s\epsilon G_{\mathrm{BU}}\left[d_{\mathrm{BU}}^{(0)}\right]^{-\alpha}}\left(1-e^{-t}\right)t^{-1-\frac{2}{\alpha}}\mathrm{d}t\right]\right)\\
&\overset{(b)}{=} \exp\left(-2\pi\lambda_{\mathrm{B}}\mathbb{E}_{\mathrm{H}}\left[\frac{(s\epsilon G_{\mathrm{BU}})^{\frac{2}{\alpha}}}{2}\left(-t^{-\frac{2}{\alpha}}\left(1-e^{-t}\right)\Big|_0^{s\epsilon G_{\mathrm{BU}}\left[d_{\mathrm{BU}}^{(0)}\right]^{-\alpha}}+\int_0^{s\epsilon G_{\mathrm{BU}}\left[d_{\mathrm{BU}}^{(0)}\right]^{-\alpha}} t^{-\frac{2}{\alpha}}e^{-t}\mathrm{d}t\right)\right]\right)\\
&= \exp\left(-\pi\lambda_{\mathrm{B}}\mathbb{E}_{\mathrm{H}}\left[(s\epsilon G_{\mathrm{BU}})^{\frac{2}{\alpha}}\gamma\left(1-\frac{2}{\alpha}, s\epsilon G_{\mathrm{BU}}\left[d_{\mathrm{BU}}^{(0)}\right]^{-\alpha}\right)-\left[d_{\mathrm{BU}}^{(0)}\right]^2\left(1-e^{-s\epsilon G_{\mathrm{BU}}\left[d_{\mathrm{BU}}^{(0)}\right]^{-\alpha}}\right)\right]\right).
\end{aligned} \tag{46}$$

$$\mathbb{E}_1 = \sum_{k=0}^{\infty}\frac{\Gamma(k+m_{\mathrm{BU}}+1)\Gamma(1-\frac{2}{\alpha})}{\Gamma(2-\frac{2}{\alpha}+k)\Gamma(m_{\mathrm{BU}})}(s\epsilon)^{k+1}d_0^{-\alpha+2-\alpha k}\left(m_{\mathrm{BU}}+s\epsilon d_0^{-\alpha}\right)^{-k-m_{\mathrm{BU}}-1}m_{\mathrm{BU}}^{m_{\mathrm{BU}}}, \tag{47}$$

$$\begin{aligned}
\mathcal{L}_{\mathrm{I_{F,2}}|_{d_{\mathrm{BU}}^{(0)},d_{\mathrm{IU},0}}} &= \mathbb{E}_{\Lambda_{\mathrm{B}}\setminus\{0\}}\left\{e^{-sH_{\mathrm{BIU}}}\right\}\Big|_{d_{\mathrm{BU}}^{(0)}} = \mathbb{E}_{\Lambda_{\mathrm{B}}\setminus\{0\}}\left\{e^{-s\epsilon^2 d_{\mathrm{BI}}^{-\alpha}d_{\mathrm{IU}}^{-\alpha}G_{\mathrm{BIU}}}\right\}\Big|_{d_{\mathrm{BU}}^{(0)}}\\
&\approx \exp\left(-2\pi\lambda_{\mathrm{B}}\int_{d_{\mathrm{IU},0}}^{D_2}\int_{d_{\mathrm{BU}}^{(0)}}^{\infty}\left(1-\mathbb{E}_{\mathrm{H}}\left[e^{-s\epsilon^2 d_{\mathrm{BI}}^{-\alpha}d_{\mathrm{IU}}^{-\alpha}G_{\mathrm{BIU}}}\right]\right)d_{\mathrm{BU}}\ \mathrm{d}d_{\mathrm{BU}}\ d_{\mathrm{IU}}f_{\mathrm{d_{IU}}}(d_{\mathrm{IU}})\ \mathrm{d}d_{\mathrm{IU}}\right)\\
&= \exp\left(-\pi\lambda_{\mathrm{B}}\int_{d_{\mathrm{IU},0}}^{D_2}\mathbb{E}_{\mathrm{H}}\left[(s\eta)^{\frac{2}{\alpha}}\gamma\left(1-\frac{2}{\alpha},s\eta\right)-\left(d_{\mathrm{BU}}^{(0)}d_{\mathrm{IU}}\right)^2\left(1-e^{-s\eta}\right)\right]f_{\mathrm{d_{IU}}}(d_{\mathrm{IU}})\ \mathrm{d}d_{\mathrm{IU}}\right),
\end{aligned} \tag{49}$$

$$\begin{aligned}
\mathbb{E}[g(\mathrm{SINR})] &= \int_0^{\infty} g(\mathrm{SINR})f_{H_{\mathrm{S}}}(x)\mathrm{d}x = \int_0^{\infty} g\left(\frac{H_{\mathrm{S}}}{\mathrm{I_F}+\delta^2}\right)\sum_{i=1}^{I}\varepsilon_i H_{\mathrm{S}}^{\beta_i-1}e^{-\xi_i H_{\mathrm{S}}}\mathrm{d}H_{\mathrm{S}}\\
&\overset{(a)}{=} \sum_{i=1}^{I}\varepsilon_i(\mathrm{I_F}+\delta^2)^{\beta_i}\int_0^{\infty} g(z)z^{\beta_i-1}e^{-\xi_i z(\mathrm{I_F}+\delta^2)}\mathrm{d}z \overset{(b)}{=} \sum_{i=1}^{I}\varepsilon_i\Gamma(\beta_i){\xi_i}^{-\beta_i}\underbrace{\int_0^{\infty} g(z)\frac{z^{\beta_i-1}}{\Gamma(\beta_i)}b^{\beta_i}e^{-bz}\mathrm{d}z}_{Q}\\
&= \sum_{i=1}^{I}\varepsilon_i\Gamma(\beta_i){\xi_i}^{-\beta_i}\int_0^{\infty} g_{\beta_i}(z)e^{-\delta^2\xi_i z}\mathcal{L}_{\mathrm{I_F}}(\xi_i z)\mathrm{d}z.
\end{aligned} \tag{50}$$

Algorithm 1 The PDF of K-Cascaded Channel Gain

Require: The mixture Gamma distribution parameters of each link: $\Theta_k: = \{\omega_{m_k}, \beta_{m_k}, \xi_{m_k}, M_k\}$, where ω_{m_k} is the weight of the m_k-th Gamma term, (β_{m_k}, ξ_{m_k}) is the parameter tuple for the m_k-th Gamma term, and M_k is the number of Gamma terms of the k-th link, $k = 1, 2, \ldots, K$, $K \geq 2$, $m_k = 1, 2, \ldots, M_k$

function CASCADE(Θ_k)
  $\mathcal{C}_{\underline{\mathbf{m}}}^{(2)} = \{1 \leq m_1 \leq M_1, 1 \leq m_2 \leq M_2, 1 \leq i \leq I\}$
  for $m_1 = 1 \rightarrow M_1$ **do**
    for $m_2 = 1 \rightarrow M_2$ **do**
      for $i = 1 \rightarrow I$ **do**
        $\varepsilon_{\underline{\mathbf{m}}}^{(2)} = \left(\prod_{j=1}^{2} \frac{\omega_{m_j} \xi_{m_j}^{\beta_{m_1}}}{\Gamma\left(\beta_{m_j}\right)}\right) \varpi_i t_i^{-\beta_{m_1}+\beta_{m_2}-1}$
        $\beta_{\underline{\mathbf{m}}}^{(2)} = \beta_{m_1}$
        $\xi_{\underline{\mathbf{m}}}^{(2)} = \frac{\xi_{m_1}\xi_{m_2}}{t_i}$
      end for
    end for
  end for
  for $k = 3 \rightarrow K$ **do**
    $\omega_{\underline{\mathbf{m}}}^{(k-1)} = \varepsilon_{\underline{\mathbf{m}}}^{(k-1)} \Gamma\left(\beta_{\underline{\mathbf{m}}}^{(k-1)}\right) \left(\xi_{\underline{\mathbf{m}}}^{(k-1)}\right)^{-\beta_{\underline{\mathbf{m}}}^{(k-1)}}$
    $\mathcal{C}_{\underline{\mathbf{m}}}^{(k)} = \{\mathcal{C}_{\underline{\mathbf{m}}}^{(k-1)}, 1 \leq m_k \leq M_k, 1 \leq i^{(k)} \leq I\}$
    for $m_{k-1} = 1 \rightarrow \mathcal{C}_{\underline{\mathbf{m}}}^{(k-1)}$ **do**
      for $m_k = 1 \rightarrow M_k$ **do**
        for $i^{(k)} = 1 \rightarrow I$ **do**
          $\varepsilon_{\underline{\mathbf{m}}}^{(k)} = \left(\prod_{j=k-1}^{k} \frac{\omega_{m_j} \xi_{m_j}^{\beta_{m_{k-1}}}}{\Gamma\left(\beta_{m_j}\right)}\right) \varpi_{i^{(k)}} t_{i^{(k)}}^{-\beta_{m_{k-1}}+\beta_{m_k}-1}$
          $\beta_{\underline{\mathbf{m}}}^{(k)} = \beta_{m_{k-1}}$
          $\xi_{\underline{\mathbf{m}}}^{(k)} = \frac{\xi_{m_{k-1}}\xi_{m_k}}{t_{i^{(k)}}}$
        end for
      end for
    end for
  end for
  return $\Theta^{(k)}: = \{\varepsilon_{\underline{\mathbf{m}}}^{(k)}, \beta_{\underline{\mathbf{m}}}^{(k)}, \xi_{\underline{\mathbf{m}}}^{(k)}, \mathcal{C}_{\underline{\mathbf{m}}}^{(k)}\}$
end function

REFERENCES

[1] A. A. Boulogeorgos et al., "Terahertz technologies to deliver optical network quality of experience in wireless systems beyond 5G," *IEEE Commun. Mag.*, vol. 56, no. 6, pp. 144–151, Jun. 2018.

[2] I. F. Akyildiz, A. Kak, and S. Nie, "6G and beyond: The future of wireless communications systems," *IEEE Access*, vol. 8, pp. 133995–134030, 2020.

[3] W. Qingqing and Z. Rui, "Towards smart and reconfigurable environment: Intelligent reflecting surface aided wireless network," *IEEE Commun. Mag.*, vol. 58, no. 1, pp. 106–112, Jan. 2019.

[4] M. Di Renzo et al., "Smart radio environments empowered by reconfigurable intelligent surfaces: How it works, state of research, and the road ahead," *IEEE J. Sel. Areas Commun.*, vol. 38, no. 11, pp. 2450–2525, Nov. 2020.

[5] Y. Han, W. Tang, S. Jin, C.-K. Wen, and X. Ma, "Large intelligent surface-assisted wireless communication exploiting statistical CSI," *IEEE Trans. Veh. Technol.*, vol. 68, no. 8, pp. 8238–8242, Aug. 2019.

[6] Y. J. Chun, S. L. Cotton, H. S. Dhillon, A. Ghrayeb, and M. O. Hasna, "A stochastic geometric analysis of device-to-device communications operating over generalized fading channels," *IEEE Trans. Wireless Commun.*, vol. 16, no. 7, pp. 4151–4165, Jul. 2017.

[7] Y. J. Chun, S. L. Cotton, H. S. Dhillon, F. J. Lopez-Martinez, J. F. Paris, and S. K. Yoo, "A comprehensive analysis of 5G heterogeneous cellular systems operating over κ–μ shadowed fading channels," *IEEE Trans. Wireless Commun.*, vol. 16, no. 11, pp. 6995–7010, Nov. 2017.

[8] Q. Wu et al., "Intelligent reflecting surface-aided wireless communications: A tutorial," *IEEE Trans. Commun.*, vol. 69, no. 5, pp. 3313–3351, May 2021.

[9] Y. Jia, C. Ye, and Y. Cui, "Analysis and optimization of an intelligent reflecting surface-assisted system with interference," *IEEE Trans. Wireless Commun.*, vol. 19, no. 12, pp. 8068–8082, Dec. 2020.

[10] X. Yu, D. Xu, Y. Sun, D. W. K. Ng, and R. Schober, "Robust and secure wireless communications via intelligent reflecting surfaces," *IEEE J. Sel. Areas Commun.*, vol. 38, no. 11, pp. 2637–2652, Nov. 2020.

[11] S. Huang, Y. Ye, M. Xiao, H. V. Poor, and M. Skoglund, "Decentralized beamforming design for intelligent reflecting surface-enhanced cell-free networks," *IEEE Wireless Commun. Lett.*, vol. 10, no. 3, pp. 673–677, Mar. 2021.

[12] A. A. Boulogeorgos and A. Alexiou, "Performance analysis of reconfigurable intelligent surface-assisted wireless systems and comparison with relaying," *IEEE Access*, vol. 8, pp. 94463–94483, 2020.

[13] D. Selimis, K. P. Peppas, G. C. Alexandropoulos, and F. I. Lazarakis, "On the performance analysis of RIS-empowered communications over Nakagami-m fading," *IEEE Commun. Lett.*, vol. 25, no. 7, pp. 2191–2195, Jul. 2021.

[14] J. Lyu and R. Zhang, "Hybrid active/passive wireless network aided by intelligent reflecting surface: System modeling and performance analysis," *IEEE Trans. Wireless Commun.*, vol. 20, no. 11, pp. 7196–7212, Nov. 2021.

[15] T. Q. Duong, H. Shin, and E.-K. Hong, "Effect of line-of-sight on dual-hop nonregenerative relay wireless communications," in *Proc. IEEE 66th Veh. Technol. Conf.*, Sep. 2007, pp. 571–575.

[16] A. K. Gurung, F. S. Al-Qahtani, Z. M. Hussain, and H. Alnuweiri, "Performance analysis of amplify-forward relay in mixed Nakagami-m and Rician fading channels," in *Proc. Int. Conf. Adv. Technol. Commun.*, Oct. 2010, pp. 321–326.

[17] K. P. Peppas, G. C. Alexandropoulos, and P. T. Mathiopoulos, "Performance analysis of dual-hop AF relaying systems over mixed $\eta - \mu$ and $\kappa - \mu$ fading channels," *IEEE Trans. Veh. Technol.*, vol. 62, no. 7, pp. 3149–3163, Sep. 2013.

[18] K. P. Peppas, "Accurate closed-form approximations to generalised-K sum distributions and applications in the performance analysis of equal-gain combining receivers," *IET Commun.*, vol. 5, no. 7, pp. 982–989, May 2011.

[19] G. K. Karagiannidis, N. C. Sagias, and P. T. Mathiopoulos, "$N*$nakagami: A novel stochastic model for cascaded fading channels," *IEEE Trans. Commun.*, vol. 55, no. 8, pp. 1453–1458, Aug. 2007.

[20] G. K. Karagiannidis, N. C. Sagias, and T. A. Tsiftsis, "Closed-form statistics for the sum of squared Nakagami-m variates and its applications," *IEEE Trans. Commun.*, vol. 54, no. 8, pp. 1353–1359, Aug. 2006.

[21] N. C. Sagias, G. K. Karagiannidis, P. T. Mathiopoulos, and T. A. Tsiftsis, "On the performance analysis of equal-gain diversity receivers over generalized gamma fading channels," *IEEE Trans. Wireless Commun.*, vol. 5, no. 10, pp. 2967–2975, Oct. 2006.

[22] H. Du, J. Zhang, K. P. Peppas, H. Zhao, B. Ai, and X. Zhang, "On the distribution of the ratio of products of Fisher-snedecor $\mathcal{F}$ random variables and its applications," *IEEE Trans. Veh. Technol.*, vol. 69, no. 2, pp. 1855–1866, Feb. 2020.

[23] N. Bhargav, C. R. N. da Silva, Y. J. Chun, É. J. Leonardo, S. L. Cotton, and M. D. Yacoub, "On the product of two κ–μ random variables and its application to double and composite fading channels," *IEEE Trans. Wireless Commun.*, vol. 17, no. 4, pp. 2457–2470, Apr. 2018.

[24] M. Di Renzo, F. Graziosi, and F. Santucci, "A comprehensive framework for performance analysis of dual-hop cooperative wireless systems with fixed-gain relays over generalized fading channels," *IEEE Trans. Wireless Commun.*, vol. 8, no. 10, pp. 5060–5074, Oct. 2009.

[25] J. G. Andrews, A. K. Gupta, and H. S. Dhillon, "A primer on cellular network analysis using stochastic geometry," 2016, *arXiv:1604.03183*.

[26] C. You, B. Zheng, W. Mei, and R. Zhang, "How to deploy intelligent reflecting surfaces in wireless network: BS-side, user-side, or both sides?" *J. Commun. Inf. Netw.*, vol. 7, no. 1, pp. 1–10, 2022.

[27] B. Zheng, C. You, W. Mei, and R. Zhang, "A survey on channel estimation and practical passive beamforming design for intelligent reflecting surface aided wireless communications," *IEEE Commun. Surveys Tuts.*, vol. 24, no. 2, pp. 1035–1071, 2nd Quart., 2022.

[28] E. Basar and I. Yildirim, "Reconfigurable intelligent surfaces for future wireless networks: A channel modeling perspective," *IEEE Wireless Commun.*, vol. 28, no. 3, pp. 108–114, Jun. 2021.
[29] H. Jiang, B. Xiong, H. Zhang, and E. Basar, "Hybrid far- and near-field modeling for reconfigurable intelligent surface assisted V2V channels: A sub-array partition based approach," *IEEE Trans. Wireless Commun.*, vol. 22, no. 11, pp. 8290–8303, Nov. 2023.
[30] R. A. DeVore and G. G. Lorentz, *Constructive Approximation*, vol. 303. New York, NY, USA: Springer, 1993.
[31] S. Atapattu, C. Tellambura, and H. Jiang, "A mixture gamma distribution to model the SNR of wireless channels," *IEEE Trans. Wireless Commun.*, vol. 10, no. 12, pp. 4193–4203, Dec. 2011.
[32] M. Abramowitz and I. A. Stegun, *Handbook of Mathematical Functions with Formulas, Graphs, and Mathematical Tables*, vol. 55. Washington, DC, USA: U.S. Government Printing Office, 1964.
[33] Q. Wu and R. Zhang, "Beamforming optimization for wireless network aided by intelligent reflecting surface with discrete phase shifts," *IEEE Trans. Commun.*, vol. 68, no. 3, pp. 1838–1851, Mar. 2020.
[34] M. Haenggi, *Stochastic Geometry for Wireless Networks*. Cambridge, U.K.: Cambridge Univ. Press, 2012.
[35] K. A. Hamdi, "A useful technique for interference analysis in Nakagami fading," *IEEE Trans. Commun.*, vol. 55, no. 6, pp. 1120–1124, Jun. 2007.
[36] H.-S. Jo, Y. J. Sang, P. Xia, and J. G. Andrews, "Heterogeneous cellular networks with flexible cell association: A comprehensive downlink SINR analysis," *IEEE Trans. Wireless Commun.*, vol. 11, no. 10, pp. 3484–3495, Oct. 2012.
[37] J. Nair, A. Wierman, and B. Zwart, "The fundamentals of heavy-tails: Properties, emergence, and identification," in *Proc. ACM SIGMETRICS/Int. Conf. Meas. Modeling Comput. Syst.*, 2013, pp. 387–388.
[38] N. C. Sagias and G. S. Tombras, "On the cascaded Weibull fading channel model," *J. Franklin Inst.*, vol. 344, no. 1, pp. 1–11, Jan. 2007.
[39] A. Abdi, "On the utility of Laguerre series for the envelope PDF in multipath fading channels," *IEEE Trans. Inf. Theory*, vol. 55, no. 12, pp. 5652–5660, Dec. 2009.
[40] I. S. Gradshteyn and I. M. Ryzhik, *Table of Integrals, Series, and Products*, 7th ed. New York, NY, USA: Academic, 2014.

Yunli Li received the B.S. degree in electronic information engineering from Nanjing University of Aeronautics and Astronautics in 2018 and the M.S. degree in telecommunications from Hong Kong University of Science and Technology in 2019. She is currently pursuing the Ph.D. degree with the Department of Electronic Engineering with the City University of Hong Kong. Her research interests include intelligent reflecting surface, channel modeling, and stochastic geometry.

Young Jin Chun (Member, IEEE) received the B.S. degree from Yonsei University in 2004, the M.S. degree from the University of Michigan in 2007, and the Ph.D. degree from Iowa State University in 2011, all in electrical engineering. From September 2011 to October 2018, he was with Sungkyunkwan University, Qatar University, and Queen's University Belfast, in various academic positions. In November 2018, he joined the City University of Hong Kong, as an Assistant Professor of wireless communication with the Department of Electronic Engineering. His research interests are primarily in the area of wireless communications, with an emphasis on stochastic geometry, system-level network analysis, device-to-device communications, and various use-cases of 5G communications.